The Antares neutrino telescope : performance studies and analysis of first data

Bruijn, R.

Publication date
2008

Chapter 3

Reconstruction

The process of reconstruction consists of finding values for the free parameters in the assumed model which most likely caused the outcome of the measurement. In the case of muon reconstruction, the basic model is a straight line passing through the detector along which a muon moves with the speed of light producing Cherenkov light on its way. The measurement consists of a set of times, positions and number of detected photons, usually referred to as hits. A commonly used reconstruction algorithm was already available, which is known as AartStrategy and documented in [74]. Alternative algorithms are also available [75], [73]. Here, a novel reconstruction algorithm will be presented that is based on a partial scan of the phase space. This algorithm is known as *ScanFit*.

3.1 Maximum Likelihood

The goal of track fitting is to find the most likely values of the parameters of the muon track $\vec{\theta}$ that caused the hits. The hits are the measurements and are denoted by $\vec{y}$. According to the *Principle of Maximum Likelihood* [57], the best estimate of $\vec{\theta}$ are the values that maximize the product of the probabilities $f(y_i;\vec{\theta})$ of the individual measurements, the likelihood :

$$L(\vec{y};\vec{\theta}) = \prod_{i=1}^{n} f(y_i;\vec{\theta}) \tag{3.1}$$

where i refers to the index of a hit. The search for the parameters $\vec{\theta}$ is in the realm of function optimisation. For practical reasons, it is customary to take the negative logarithm of the likelihood and perform a minimisation on its value. This can be done using custom made algorithms or by making use of an existing software package. In this work both approaches are used. The software package used is MINUIT [76].

The existence of multiple (local) maxima of the likelihood can not be excluded. In addition, symmetries can introduce solutions in different parts of the parame-

ter space that are equally correct, given the same measurements. So, care should be taken of two things. First, the common optimisation algorithms are guided through parameter space by gradients and second derivatives, and thus follow a certain path. When the starting conditions are unfavorable, certain parts of the parameter space will remain unexplored, possibly containing the global maximum of the likelihood. In case there are different solutions which have the same value of the likelihood, they should all be found. The way these two points are taken care of, is by making sure the whole parameter space is explored.

The likelihood used in this work is primarily defined as the product of the probabilities of time t_i of a hit i. The probability of measuring a certain hit time depends strongly on the track parameters. Given the measured time of a hit t_i and the model prediction of the hit time t_i^{th}, the time residual $t_i - t_i^{th}$ can be determined. The probability of measuring a hit with a certain residual is described by a Probability Density Function (PDF)

3.1.1 Probability Density Function

As explained in section 2.5 the photons that are detected are not only caused by direct Cherenkov emission from the muon. Excluding these effects, the PDF of the measured arrival times of photons can be approximated by a Gaussian distribution. The contribution from other processes and the scattering of light introduces a time delay with respect to the hypothesized direct Cherenkov light, as will be shown below. A complete model of a muon should include the positions and energies of electro-magnetic showers along the track. Due to the stochastic nature of these processes the number of parameters would then vary. The way this is usually handled is to include the averaged effects into the PDF. In this, the correlated effects between different hits are neglected. The exact modeling of such a PDF requires reliable knowledge about the contributing processes. These include the knowledge of the involved cross sections, the water parameters like scattering and absorption lengths, and a complete knowledge of the detector response.

3.1.2 The Gaussian approximation

Another approach is to enhance the purity of the measurements with respect to the assumed hypothesis. In the case of muon reconstruction, the hypothesis is that light is emitted from a muon at the Cherenkov angle. In that case, the PDF can be approximated by a Gaussian distribution. When the PDF of the hit-time residuals can be described by a Gaussian distribution with a width σ_i, the likelihood can be expressed as

$$L(\vec{t};\vec{\theta}) = \prod_{i=1}^{n} \frac{1}{\sqrt{2\pi}\sigma_i} e^{-\frac{1}{2}\left(\frac{t_i - t_i^{th}(\vec{\theta})}{\sigma_i}\right)^2} \tag{3.2}$$

Taking the logarithm of this equation yields

$$l(\vec{t};\vec{\theta}) = -\frac{n}{2}\ln 2\pi + \sum_{i=i}^{n} - \ln\sigma_i - \frac{(t_i - t_i^{th}(\vec{\theta}))^2}{2\sigma_i^2} \tag{3.3}$$

Maximizing L is now equivalent to minimizing

$$\chi^2(\vec{t};\vec{\theta})/2 = \sum_{i=1}^{n} \frac{(t_i - t_i^{th}(\vec{\theta}))^2}{2\sigma_i^2} \tag{3.4}$$

The χ^2 is a quantity with well-known properties [57]. One of the advantages is the possibility to use a χ^2 test, which is a way of assessing the goodness-of-fit. It relies on the known distribution of the χ^2 values for a given number of degrees of freedom, n_{dof}. This number amounts to the number of hits minus the number of free parameters in the fit, $n_{dof} = n - n_{par}$. The χ^2 probability corresponds to the likelihood that with a correct model and Gaussian errors, the χ^2 has a value equal or larger than the one obtained, given the number of degrees of freedom.

3.1.3 M-estimator

The χ^2 fitting procedure can be sensitive to so-called outliers. Outliers are hits with large residuals, either negative or positive. The derivative of the χ^2 with respect to the residuals depends linearly on the residual. This causes the weight of an outlier to increase linearly with the value of the residual. To reduce the influence of outliers, a different quantity can be minimized

$$M = \sum_{i=1}^{n} \rho(\frac{t_i - t_i^{th}}{\sigma_i}) \tag{3.5}$$

Where

$$\rho(z) = \ln(1 + \frac{1}{2}z^2) \tag{3.6}$$

This function behaves as the χ^2 function for small residuals. But for large residuals, the χ^2 depends logarithmically on the residual. As a consequence, large residuals have less influence, and the fit result depends less on the few outliers present in the measurement.

3.2 Parameters

In the general case, 5 parameters can describe the muon track. The direction of the muon can be described by the zenith angle (θ) and azimuth angle (ϕ). These

angles can be used to define a rotation of the coordinate system. The axes of the new coordinate system are then given by $\vec{x}' = \mathbf{R}\vec{x}$, where

$$\mathbf{R} = \begin{pmatrix} \cos(\theta)\cos(\phi) & \cos(\theta)\sin(\phi) & -\sin(\theta) \\ -\sin(\phi) & \cos(\phi) & 0 \\ \sin(\theta)\cos(\phi) & \sin(\theta)\sin(\phi) & \cos(\theta) \end{pmatrix} \tag{3.7}$$

The topology is shown in figure 3.1. In the new coordinate system the z-axis points in the direction of the muon. The $z' = 0$ plane is perpendicular to the muon direction. The point at which the muon crosses this plane is given by the parameters a and b. Finally, the time at which the muon crosses the plane $z' = 0$, is referred to as t_0. In summary, the five parameters describing the muon are θ, ϕ, a, b and t_0. Sometimes the angles θ and ϕ are replaced by the unit three-vector $\hat{d} = (\sin(\theta)\cos(\phi), \sin(\theta)\sin(\phi), \cos(\theta))$.

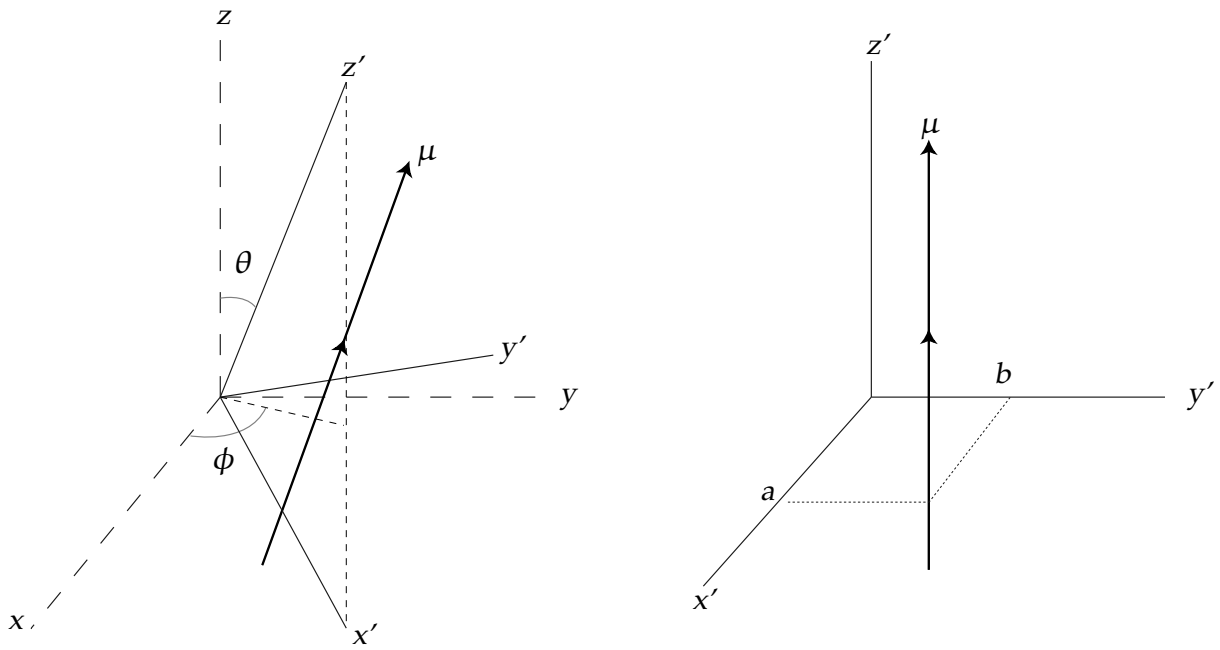

Figure 3.1: *The muon direction is given by θ and ϕ which define a rotation of the coordinate system. The position of the muon track is then defined by the transverse coordinates a and b in the rotated system.*

From the track parameters and the position of a PMT ($\vec{x}$), the arrival time of a photon can be determined. A coordinate system in which the z-axis lies along the muon direction can be obtained by rotating the coordinate system using the given zenith angle θ and azimuthal angle ϕ of the muon. The rotated position of the PMT is $\vec{x}'$. The arrival time of the photon (figure 3.2) can then be expressed as

:

$$t_j = t_0 + \frac{1}{c}\left(z'_j - \frac{r_j}{\tan(\theta_c)}\right) + \frac{1}{v_g}\frac{r_j}{\sin(\theta_c)} \tag{3.8}$$

with z'_j the z-coordinate of the PMT in the rotated frame, $r_j = \sqrt{(a-x')^2 + (b-y')^2}$ the 2D distance between the track and PMT, θ_c the Cherenkov angle and v_g the group velocity of light in water (see figure 3.2).

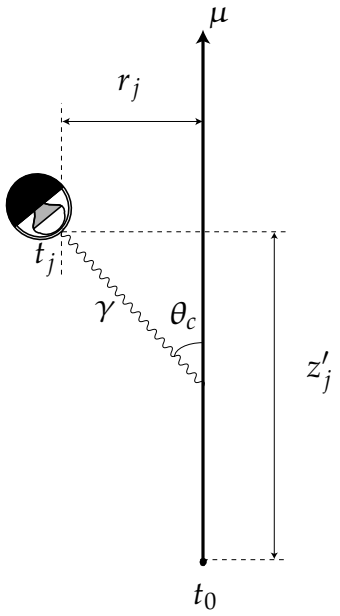

Figure 3.2: *Schematic view of a muon passing an optical module*

3.3 Hit Selection

3.3.1 L1′ Hits

A photon hitting a photomultiplier tube is digitized when the analogue signal from the anode exceeds a certain threshold, typically set at 0.3 photo-electron equivalent charge. The corresponding digital data are referred to as a L0 hit. A local coincidence of L0 hits on the same storey constitutes a L1 trigger. The coincidence gate is usually set at $[-20\text{ ns}, +20\text{ ns}]$. Also a hit with a large amplitude can be considered an L1 trigger. The amplitude has to be larger than a value, a_{th}, referred to as the high-amplitude threshold, and has a typical value of 3 photo-electrons. This value is set to suppress hits from the tail of the 1 photo-electron peak. In this work, single L0 hits are only used if they have an amplitude of at least 0.5 photo-electron. A L1′ hit is defined as the first hit of a L1 trigger. A L1′ hit has a higher probability of being due to direct Cherenkov light from a

muon track, as scattered photons and photons from EM-showers, in general, arrive later than photons from the direct Cherenkov light. To see this, consider a photon emitted from a random point along a track. The arrival time is given by replacing θ_c in formula 3.8 by an angle θ with $0 < \theta < 180°$. This yields

$$t_j = t_0 + \frac{1}{c}\left(z_j - \frac{r_j}{\tan(\theta)}\right) + \frac{1}{v_g}\frac{r_j}{\sin(\theta)}. \tag{3.9}$$

By subtracting 3.8 from 3.9 one obtains the time difference Δt between a Cherenkov photon and a photon emitted somewhere along the track in the direction of the PMT. After some manipulation, this results in

$$\Delta t = \frac{r_j}{c}\left(\frac{1 - \cos(\theta_c - \theta)}{\sin\theta\cos\theta_c}\right). \tag{3.10}$$

The value of Δt has a minimum of 0 at $\theta = \theta_c$ and is positive for any other value of θ. A photon emitted under the Cherenkov angle has the shortest optical path.

3.3.2 1D Clustering

As explained in 2.8 the standard trigger algorithm [72] looks for clusters of space-time correlated hits. Hits are causally related if they satisfy the causality relation 2.8.

In the framework of gamma-ray burst studies, a directional trigger was developed [47]. This trigger makes use of a more restrictive causality criterion. This is possible by using the information on the direction of the muon. When the coordinate system is rotated in such a way that the z-axis lies along the assumed direction of the muon, the expected arrival time t_j of a photon on a PMT can be expressed as in equation 3.8. Using $\kappa = \frac{c}{v_g}\frac{1}{\sin\theta_c} - \frac{1}{\tan\theta_c}$ this equation simplifies to

$$t_j = t_0 + \frac{1}{c}(z_j + \kappa r_j). \tag{3.11}$$

When considering two hits at times t_i and t_j (see figure 3.3) and by taking the time difference, one obtains after some manipulation

$$c(t_j - t_i) - (z_j - z_i) = \kappa(r_j - r_i). \tag{3.12}$$

The value $r_j - r_i$ is maximal and equal to the 2D distance R between the hits R when the muon track crosses either PMT. So

$$-R \leq r_j - r_i \leq R \tag{3.13}$$

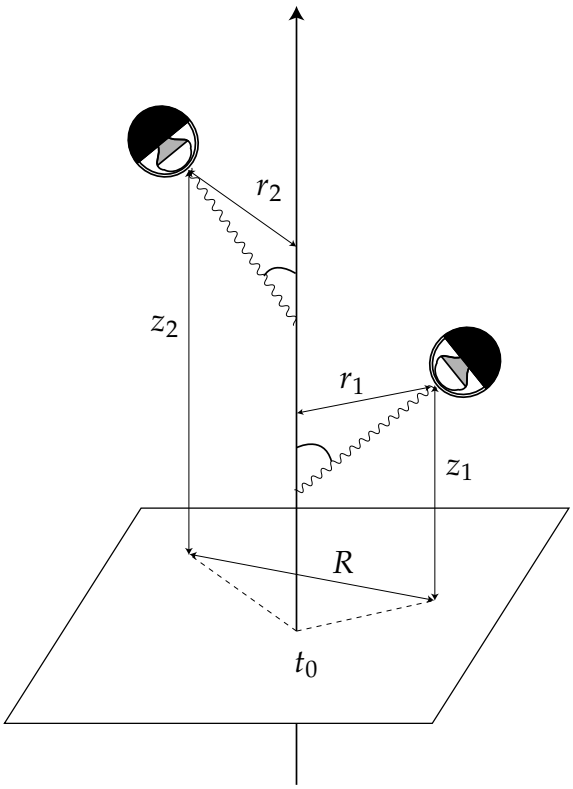

Figure 3.3: *Schematic view of a muon passing two optical modules.*

and thus the condition for two hits to be related becomes

$$-\kappa R + (z_j - z_i) \leq c(t_j - t_i) \leq \kappa R + (z_j - z_i) \tag{3.14}$$

This relation is more restrictive as the maximal time difference is determined by the the 2D distance between the PMTs. The distance along the assumed track direction is taken into account as the propagation time of the muon. In practice a safety margin of 20 ns is added, in order to account for effects of electronics, light scattering and inaccuracies in the alignment of the detector. The algorithm that is described below was designed to be applied to the first data taken with the Antares detector. In that phase, accurate alignment was not yet available. Therefore the safety margin is also used in the fit algorithm. With a more accurate alignment of the detector, the safety margin could be reduced.

An additional restriction when matching pairs of hits comes from the attenuation of the intensity of the Cherenkov photon flux. The photon intensity is described by formula 2.7. This means that most photons from the muon will be detected within a certain roadwidth from its path. By cutting on a maximum 2D distance between hits, the background of accidental coincidences will be reduced. As can be inferred from equation 3.14, the probability of an accidental coincidence increases with this distance. An additional condition is :

$$|r_j - r_i| < R_{max} \tag{3.15}$$

The value of R_{max} is usually set to a value corresponding to two attenuation lengths.

3.4 Track Reconstruction

For the fitting method that has been developed in this work, a selection of the hits is made using L1′ hits and directional clustering. The fitting algorithm basically consists of three steps :

1. **Scanning**
   A scan over a part of the parameter space is made. For each point in the sub-space, a hit selection is made and the selected hits are used to make a prefit. The result is a set of prefits with associated hits.

2. χ^2 **fit**
   In this phase a χ^2 fit is made to determine final track parameters, using the prefits as start values. The hits which were selected in previous phase are used. Hits that are incompatible with the improved fit could be removed.

3. **Track Ordering**
   As, in general, the result is a set of track candidates, the tracks are ordered.

3.4.1 Scanning

The scanning phase is designed to tackle several problems inherent to the track fit. The first is the problem of the starting value. As the track fit is a non-linear problem (see equations 3.7 and 3.8), it has to be solved through an iterative process in which values for the track parameters are sought which maximize a likelihood or minimize a χ^2. Such a procedure requires a starting value for each of the parameters. However, it can be shown [77] that when assuming a direction, the determination of the remaining parameters can be reduced to a linear problem when only direct Cherenkov hits are considered. As a consequence, for each direction there is a unique solution for the position and time of the track. Another problem is the possibility of local maxima of the likelihood. This means that one can end up in a region of the parameter space where the derivatives of the likelihood are zero. Eventually, a local minimum could be considered as a solution. By scanning over the angular space, the local maxima are mapped out and no part of the phase space is missed. An important aspect of χ^2 minimisation, is finding the right hits. For this, the 1D clustering is used. To do the scan, the angular space (covering solid angle Ω) is divided in a grid with n_g points, distributed isotropically. This gives a set of points $G = \{(\theta_0, \phi_0), (\theta_1, \phi_1), ..., (\theta_{n-1}, \phi_{n-1})\}$. For each point, the directional clustering algorithm is applied to the L1′ hits. This yields a cluster of L1's of size $n_{L1'}$. If $n_{L1'} \leq n_{par}$,with n_{par} the number of free parameters in the fit, this direction is rejected. Until now, only L1′ hits are considered. These form a subset of the muon hits. Single L0 hits are not included. However, these form a significant fraction of the number of muon hits. In order to enhance the

hit yield, L0 hits are added to the sample. A L0 hit is added if it is causally related, assuming the given direction, with each selected L1' hit. Furthermore, the added L0's have to be causally related with each other. The total number of hits associated with a given direction is referred to as n_{tot}.

Prefit

In order to supply the following fitting steps with sufficient information, the position and time of the muon should be determined for each assumed direction. These quantities are estimated in several steps. Even though the problem is linear for a given direction, the estimation is done iteratively. The reason for this is that it allows the use of a *M-estimator* PDF. First, this takes care of a non 100% pure hit selection. Secondly, as the direction is quantized with a grid size Ω/n_g, the closest grid point can be some degrees away from the true track direction.

Linear approximation As a start, the position of the track is estimated by taking the average of the hit positions in space. From this, using the Cherenkov hypothesis, t_0 is calculated for each hit. The average of these values is used for the t_0 of the track. These two steps are repeated, but the hit coordinates perpendicular to the track are weighted using an estimated transverse distance.

Powell's Method Subsequently, the hit-time residuals are minimized using Powell's method ([58]). In short, this procedure carries out successive 1-dimensional gradient-less line-minimisations on a set of vectors in the 3-dimensional parameter space. This set of vectors is continuously optimized to achieve quick convergence, by including the vector difference between the previous point and the current point after each minimisation step.

Marquardt Method Previous procedures are used to get sufficiently close to the minimum of the function to be minimized. When this is the case, the function can be approximated by a quadratic form :

$$\chi^2(\vec{\theta}_{min}) \simeq \chi^2(\vec{\theta}_i) - (\vec{\theta}_{min} - \vec{\theta}_i) \cdot \nabla\chi^2(\vec{\theta}_i) + \frac{1}{2}(\vec{\theta}_{min} - \vec{\theta}_i) \cdot H \cdot (\vec{\theta}_{min} - \vec{\theta}_i) \tag{3.16}$$

Where $\vec{\theta}_i$ ($\vec{\theta}_{min}$) is the 3-vector containing the position and time at current iteration (minimum), $\nabla\chi^2(\vec{\theta}_i)$ its gradient and H is the Hessian matrix, containing the second derivatives. In this case, the minimisation can be made in all 3 dimensions simultaneously :

$$\vec{\theta}_{min} = \vec{\theta}_i + H^{-1} \cdot [-\nabla\chi^2(\vec{\theta}_i)] \tag{3.17}$$

This method can be applied when the Hessian matrix can be calculated analytically, which is the case for a χ^2 or *M-estimator* PDF. When far away from

the minimum or if the approximation 3.16 is not valid, only a step along the gradient can be taken :

$$\vec{\theta}_{new} = \vec{\theta}_i - constant \times \nabla\chi^2(\vec{\theta}_i) \tag{3.18}$$

The constant should be sufficiently small so as not to step over the minimum. Marquardt's method [58] uses a continuous steering parameter λ for which the value depends on the success of the last minimisation step.

Not all prefits yield equally good candidates. For reasons of efficiency in the following steps, an ordering of the prefits is helpful. The prefits can be sorted according to the number of associated hits N_{tot}. This is based on the assumption that for a direction close to the true direction, most hits should be found using the cluster procedure described above.

3.4.2 χ^2 Fit

The goal of the previous scanning phase is twofold. First it supplies a number of candidate directions, together with estimates of the position and time coordinates. Secondly, for each of the directions it includes a set of hits. In the final fit, also the direction is fitted, hence, the effect of the discretisation of the direction on the expected hit-time residual is no longer present. As a consequence, the fit is more demanding in terms of cpu-time. For performance reasons, the smallest clusters can be rejected. The largest number of associated hits is N_{max}. Only candidates with N hits are considered where $N > (1 - P_{Ncut}) \times N_{max}$. When the intrinsic time resolution is assumed in the calculation of the χ^2, the influence of impurities, or outliers, increases. This influence is twofold. First, outliers can pull the fit, so that the minimum of the χ^2 doesn't correspond to an accurate estimate of the track parameters. Secondly, events with outliers are more likely to be rejected on basis of their χ^2 probability, even though they can have a reasonable estimate of track parameters. In order to increase reconstruction efficiency and accuracy, the possibility to remove outliers is included. Outlier removal is attempted if the χ^2 probability of a fit is smaller than a value P_{min}. If the value of the probability is dominated by one or few outliers, removal of the outliers is beneficial. One outlier is removed at a time, and a fit is made with the remaining hits. The hit to be removed is the one contributing the most to the χ^2 and for which $\Delta t \geq n_{stdev} \times \sigma$. The number of standard deviations n_{stdev} is typically set to a value of 5. The final fitting procedure can be described as follows : First, the track parameters are fitted using a M-estimator PDF. Secondly, the χ^2 probability is calculated and, if it is below P_{min}, hit removal is attempted, until either the probability exceeds P_{min} or the maximum number of hits has been removed or no hit can be removed.

3.4.3 Track Selection

In the final step all parameters are left free to be estimated. Therefore the possibility exists that fits with different starting values from prefits converge to approximately the same solution. These tracks are identified as identical if the difference is less than some degrees. This value should be in the order of the final angular resolution of the fitting procedure. The collection with identical solutions is then sorted based on number of hits, and χ^2. For a given direction, the fit with the largest number of hits is preferred. If there are multiple solutions with the same number of hits, the one with the smallest χ^2 value is taken. The final result consists in the general case of multiple solutions. As mentioned earlier, multiple solutions are a consequence of symmetries in the topology of the event and the detector geometry. In general, ambiguities can not be excluded. The way to handle these depends on the kind of analysis. One way is to exclude events that have multiple solutions. This, of course, affects the detection efficiency, as it will cut away signal and introduce a bias. The other option is to keep these events and to take the solution that is most likely, according to some criterion. This is similar to commonly used reconstruction procedures which try to find a single solution. An interesting option is to use all solutions for point-source searches.

3.4.4 1 Dimensional case

A special case occurs when all the hits lie on a straight line. This is the case when hits are recorded on a single detector string. This implies a rotational symmetry around that axis. Consequently, the ϕ angle cannot be determined from the data. There is no need to scan over ϕ, and it can be set to a fixed value, arbitrarily chosen to be 0. There is now one parameter less to be fitted. This special case will be treated more in-depth in chapter 4.

3.5 PDF fit

In the described fit procedure the philosophy is to select those hits with a high purity with respect to the Cherenkov hypothesis. The ultimate fitting procedure should include all available information and thus use all hits. In order to asses the full potential of the reconstruction, a designated PDF fit can be done. So, the reconstruction algorithm described until now, ScanFit, acts as input to this fit. The PDF that is used has been developed in [74] and is implemented in the final fitting stage of the full reconstruction procedure. This PDF describes the probability for a hit-time residual Δt. Two additional effects are taken into account :

1. The rate of random background hits with amplitude a is given by $R^{bg}(a)$. In order to be able to normalize the PDF, only a finite time window is considered. The random hits are assumed to be distributed uniformly between

$-T/2$ and $T/2$, and each value of Δt is thus equally probable. The value of T is chosen large enough to contain all the signal hits. It typically amounts to 500 ns.

2. The PDF for the signal hits describes the distribution of the time residual Δt between the arrival time of a detected photon and a hypothesized Cherenkov photon. The PDF also includes effects from other processes like electro-magnetic showers. The PDF depends on the amplitude a of a hit. The probability of measuring a residual Δt is then expressed as $P^{sig}(\Delta t|a)$.

The relative contributions of the signal and background probabilities depend on several quantities. The main two quantities are the distance traveled by the photon to the optical module (d), and the angle of incidence of the photon on the optical module (α). These quantities can be determined from the track parameters, assuming the photon is emitted at the Cherenkov angle. The expected number of signal hits for a given amplitude $N^{sig}(\alpha, d|a)$ depends on these quantities. This value, together with the expected number of background hits is used to weight the time residual probabilities :

$$P(\Delta t|\alpha, d, a) = \frac{P^{sig}(\Delta t|a)N^{sig}(\alpha, d|a) + R^{bg}(a)}{N^{sig}(\alpha, d|a) + R^{bg}(a)T} \tag{3.19}$$

where the denominator corresponds to the expected total number of hits. $N^{sig}(\alpha, d|a)$ can be factorized in two different components, the expected number of hits which depends on distance and a factor describing the angular acceptance of the optical module, which depends on the angle of incidence :

$$N^{sig}(\alpha, d|a) = N(d|a) \times f(\alpha|a) \tag{3.20}$$

Both terms are obtained by fitting an appropriate function to the distributions obtained from simulations that include light scattering, shower processes etc. These distributions are made for different bins of amplitude. The chosen bin edges are $0, 1.5, 2.5, 5, 10$ and ∞ photo-electrons. For a detailed description of the distance and angle parameterisations, see [74]. Due to the amplitude dependence of the TTS of the PMT, there is a relation between the shape of $P^{sig}(\Delta t|a)$ and the variables d and α. However, $P^{sig}(\Delta t|\alpha)$ is not explicitly dependent on these two variables. The relation is implicitly taken into account by dividing both $P^{sig}(\Delta t|\alpha)$ and $N^{sig}(\alpha, d|a)$ into the same bins of amplitude. The muon energy has been integrated over.

Hit-Time Residual PDF

The likelihood as defined in formula 3.1 assumes uncorrelated hit probabilities. However, this is not necessarily the case. When the duration of the photon flux on a PMT exceeds the integration gate of the ARS, the second ARS takes over,

and a second hit is recorded (see section 2.6.3). In this case, the second hit is correlated with the first one and doesn't contain extra information. These second ARS hits cause the additional, off-zero peak in the hit-time residual distribution. The original $P^{sig}(\Delta t|a)$ doesn't account for this correlation and all hits are used in the calculation of the likelihood of the fit. On the other hand, a parameterisation for $P^{sig}(\Delta t|a)$ was made which ignores the double peaked structure. The reason for this was to avoid additional local minima in the likelihood. The parameterisation describes $P^{sig}(\Delta t|a)$ for a given amplitude bin, by a single Gaussian peak and a tail, parameterised as $C_{tail}e^{-\Delta t/\eta}/(\Delta t + \rho)$. The peak and tail are joined by a third-power polynomial in the range $c_1 \leq \Delta t \leq c_2$, requiring that the function is continuous and differentiable at the points c_1 and c_2. Including c_1 and c_2, the total number of free parameters in the function is 12. The values of the parameters are determined by fitting the function to normalized distributions of time residuals, obtained from a simulation of the detector response.

In this work, a different approach has been made in order to remove the above mentioned correlation. This is done by removing the hits that are recorded in the second ARS immediately after the integration gate of the first closes. This is accomplished by introducing a virtual dead-time after each hit, with a duration somewhat larger than the ARS integration gate. The above described parameterisation $P^{sig}(\Delta t|a)$ is then fit to the new distributions. The resulting distributions for the different amplitude bins are shown in figure 3.4. It can be seen from figure 3.4 that the peak due to the second ARS hits has disappeared, though a small remnant can be noticed. The peak at zero is unaffected by the dead-time, and the fits are generally very good.

3.6 Performance

In this section the performance of the reconstruction algorithm will be summarized. As explained above, the algorithm is divided in several phases. The behavior of each of these phases is presented separately. The combined result will also be given. The performance is tested on simulated data, so that the true values of the parameters to be estimated are known. An important parameter to measure is the pointing accuracy of the telescope. To measure the pointing accuracy, a quantity is introduced :

$$\Delta a_\mu = \cos^{-1}(\hat{d}_\mu^{true} \cdot \hat{d}_\mu^{fit}) \tag{3.21}$$

With $\hat{d}$ as defined in section 3.2. It measures the angular error between the true muon and the reconstructed muon (3.21). The data set consists of muons originating from upward going neutrinos. The neutrinos were generated with an energy spectrum $\frac{dN}{dE} \propto E^{-1.4}$ in the range from 10 GeV to 10^7 GeV. The detector response depends on the energy of the muon. Therefore, some quantities are presented as a function of the muon energy. A study on the effect of the random background

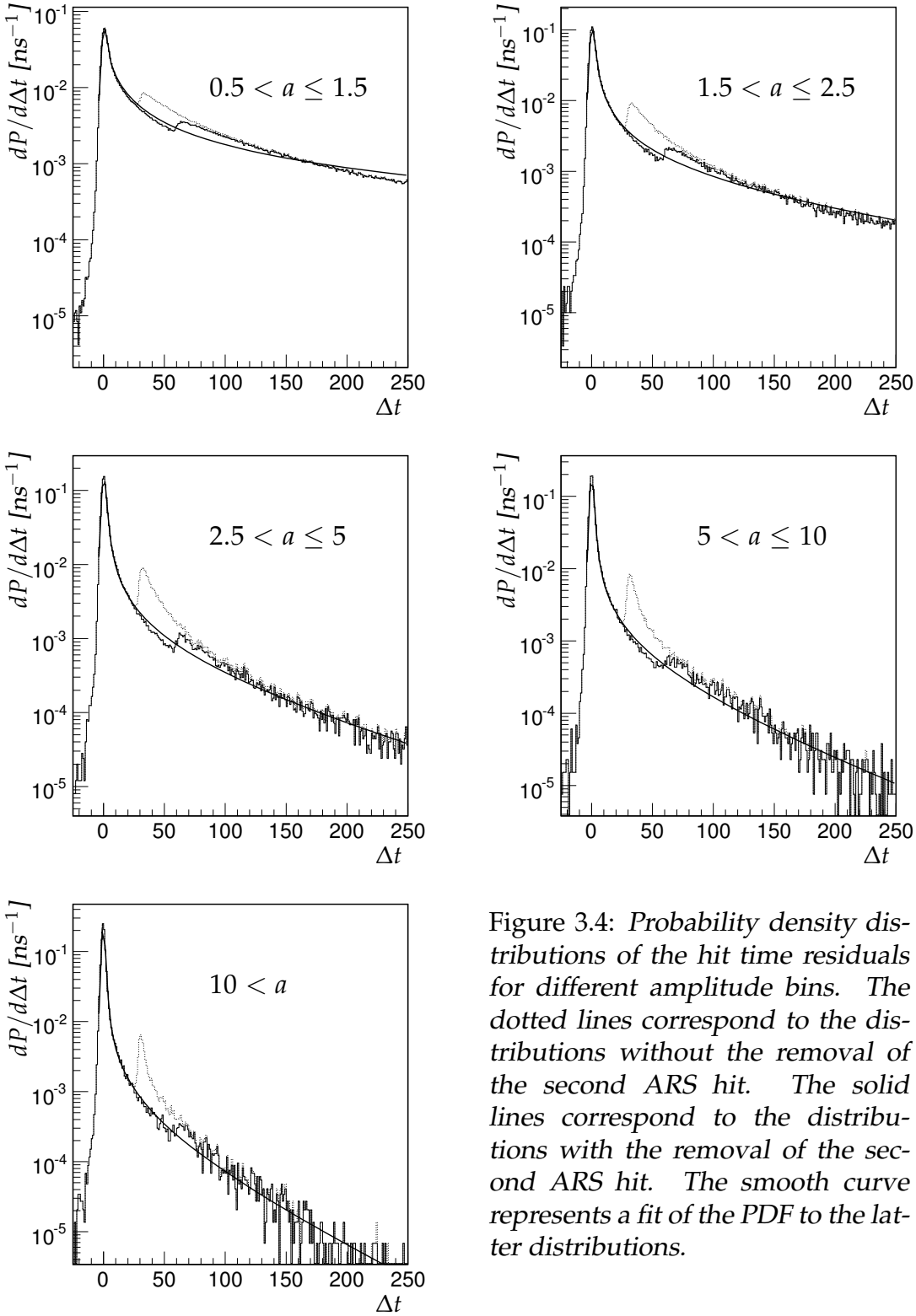

Figure 3.4: *Probability density distributions of the hit time residuals for different amplitude bins. The dotted lines correspond to the distributions without the removal of the second ARS hit. The solid lines correspond to the distributions with the removal of the second ARS hit. The smooth curve represents a fit of the PDF to the latter distributions.*

is included. For this purpose three levels of background are considered : 60 kHz, 120 kHz and 240 kHz. This largely covers the background observed so far. For some studies, the hypothetical case of no background is also included.

3.6.1 Hit Selection

As described in section 3.3, the selection of hits is based on a 1-dimensional causality criterion. In order to enhance purity a maximum transverse distance between two hits is imposed. In figure 3.5 the distributions of the transverse distance are shown. With increasing rates, the contribution of background to the L1' sample increases at larger distances. The reason for this can be found in formula 3.14. The allowed time interval increases with distance, and so does the probability for two random hits to coincide. Also, the effect of using L1'-hits can be seen by comparing the left and right plots. When using the L1'-hits, the obtained distributions overlap up to 90 meters, which represents 85 % of all signal hits. When using L0's the distributions differ significantly. A maximal value of the transverse distance has been introduced in section 3.3.1. Due to the geometry of the detector, the number of PMTs contained in a cylinder with radius R depends on the zenith angle θ. This is taken into account by making the value of R_{max} depend on the zenith angle :

$$R_{max}(\theta) = R_{max} \times (1 - 0.25\cos^2(\theta)) \tag{3.22}$$

The value of R_{max} is set to 90 meters.

Purity and Efficiency

The purity and efficiency of the hit selection determine the quality of reconstruction. The main reason for this is that the background is not modeled in the χ^2 fit. The purity of the hit-selection is defined as the fraction of the selected hits that is truly caused by a muon. A purity of 1 (or 100 %) indicates that no background hits are included. No distinction is made between photons due to Cherenkov light or due to electro-magnetic showers. The efficiency is defined as the ratio of the number of storeys in the selection and the total number of storeys that recorded a photon from the muon. It is defined in this way because at most one hit from a storey is used. Figures 3.6 and 3.7 summarise the purity and efficiency of the hit-selection in the simulated sample. Both the purity (figure 3.6, left) and the efficiency (right) are found to be independent of zenith angle. This supports the definition of $R_{max}(\theta)$ given in equation 3.22. Both purity and efficiency depend on the background rate, as can be expected. At 240 kHz the overall purity of the sample is above 90% and at 120 kHz above 95%. The overall efficiency remains above 40%. The maximum efficiency is about 50 %. When considering the muon energy dependence of both the purity (figure 3.7, left) and efficiency (figure 3.7,

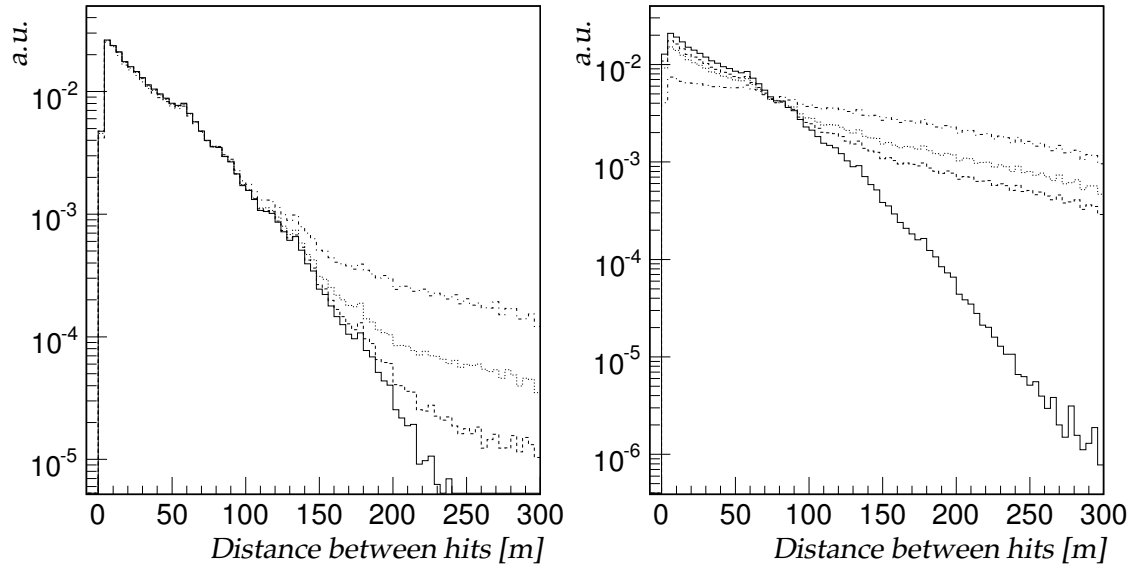

Figure 3.5: *Distributions of transverse distances between pairs of hits, corrected for phase-space effects. Left plot shows the distribution for L1′ hits, the right plot shows the distribution for the remaining L0 hits. Line type indicates background rates. The solid line represents no background. The dashed line represents a background rate of 60 kHz, the dotted line 120 kHz and the dash-dotted line 240 kHz.*

right), larger differences are observed. For any background rate, the purity decreases toward lower energies, and increases with increasing energy. The purity exceeds 95% for energies in excess of 100 TeV. The efficiency without background drops from about 70% at 10 GeV to just above 20% at 10 PeV. The explanation for this strong energy dependence lies in the increased photon yield with increased energy. On one hand it increases the purity, as the relative contribution of background hits decreases. On the other it decreases the efficiency as the additional hits more likely originate from electro-magnetic showers. These hits do not always satisfy the 1D causality criterion. The dependence of the efficiency on the background rate at low energies is caused by the interference of background hits which can cause signal hits to be rejected.

When the assumed muon direction deviates from the true muon direction, less hits are expected to be causally related. This affects the efficiency of the hit-selection. This loss in efficiency manifests itself in two ways. The first is a reduction of events which have enough hits to make a (pre)fit. The second is a general reduction of the number of hits. Both effects are studied as a function of the deviation of the assumed muon direction from the true muon direction.

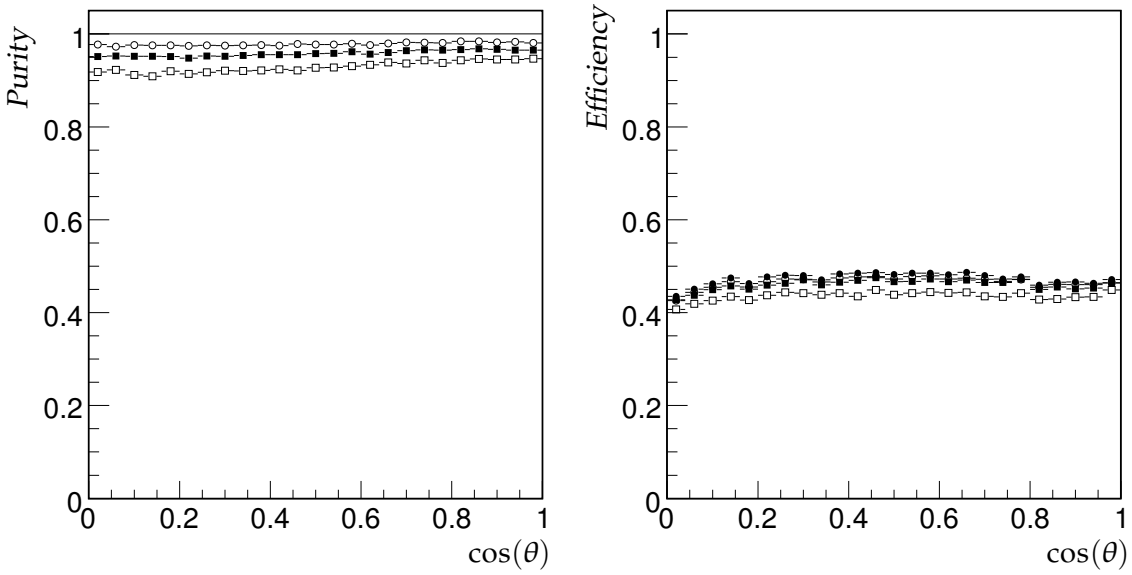

Figure 3.6: *Left : The purity of the hit selection as a function of the cosine of the zenith angle of the muon direction. Right : The efficiency of the hit selection as a function of the cosine of the zenith angle of the muon direction. The solid line is without background, the open circles indicate a background of 60 kHz, the closed squares indicate a background of 120 kHz and the open squares indicate a background of 240 kHz.*

The results are summarised in figure 3.8. The reconstruction efficiency is defined as the fraction of the total events that has sufficient hits ($\geq$ 5) for a (pre)fit. The hit selection efficiency is defined as the fraction of hits that remain. Up to 20 degrees, the reconstruction efficiency shows a plateau at about 95 %, while the hit-efficiency (figure 3.8, right) shows a large negative gradient. In this region, the fit quality is expected to decrease due to the reduction of the number of hits. Above 20 degrees, the reconstruction efficiency begins to fall, and the drop in the hit efficiency begins to flatten. This implies that the events that survive have just enough hits.

Hit time residuals

As mentioned earlier, the goal of the hit selection is to increase the purity with respect to the assumed muon hypothesis. This includes suppressing the late hits from the electro-magnetic showers and the hits from the continuous background. In the previous section, the purity with respect to the background and efficiency has been evaluated. This was done without making a distinction between the

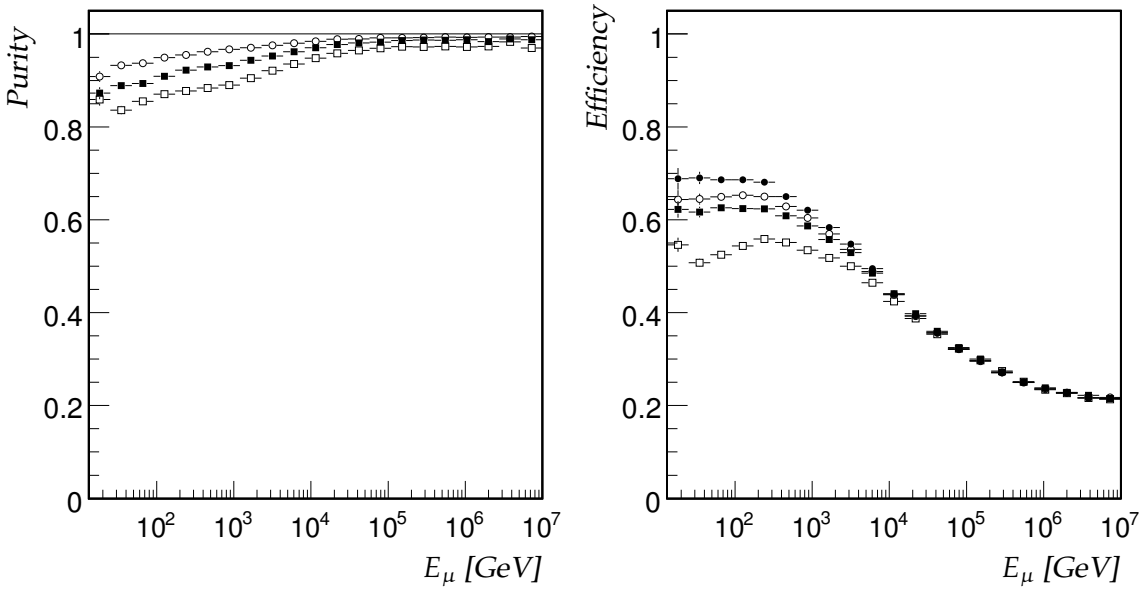

Figure 3.7: *Left : The purity of the hit selection as a function of the muon energy. Right : The efficiency of the hit selection as a function of the muon energy. The solid line is without background, the open circles indicate a background of 60 kHz, the closed squares indicate a background of 120 kHz and the open squares a background of 240 kHz.*

origin of the hit, which could be either direct Cherenkov or an electro-magnetic shower. When considering only direct Cherenkov light from a muon, the latter contribution should be suppressed as well. The tail of late hits should then decrease and the overall distribution should become more Gaussian. This aspect of the hit selection has been studied by comparing hit time residual distributions before and after the hit selection. In order to disentangle the effects of background and muon energy, the comparison is done for the different background rates and muon energies. The contribution of hits in the second ARS peak is suppressed by favoring the first L1 trigger in an LCM, be it either a coincident pair or a high amplitude hit. This is done by introducing a virtual dead-time after a L1 trigger, with a duration larger than the ARS integration gate. Figure 3.9 shows the distributions of time residuals for various conditions. The energy ranges are 10 GeV - 1 TeV, 1 TeV - 100 TeV and 100 TeV - 10 PeV. These ranges are chosen to represent a regime with low contribution from showers, the onset of a significant shower contribution and a shower dominated regime, respectively . In each plot, the distribution of hit time residuals before selection and after selection is shown. The latter corresponds to the hit sample that is used for the prefit and the subsequent χ^2 fit. Both distributions are normalized to retain the relative probabilities. The

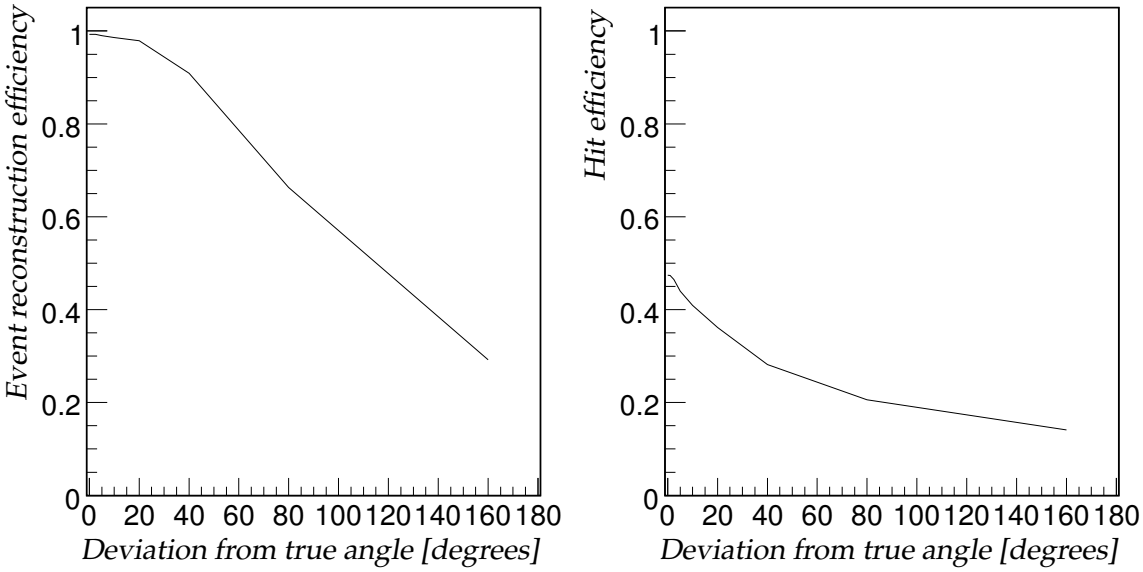

Figure 3.8: *Left : Efficiency to reconstruct an event as a function of the deviation of the assumed angle from the true muon angle. Right : Hit collection efficiency as a function of the deviation of the assumed angle from the true muon angle*

difference at a given residual is equal to a reduction of hits. As can be seen from figure 3.9 the tail of the distribution is suppressed, and the distribution resembles more closely a Gaussian distribution by making a hit selection. A feature is the increasing contribution of the second ARS peak with increasing rate. This is most clearly seen at the highest energies. This effect occurs even though the first hits are selected. It is due to the increased probability of a random hit preceding a high amplitude hit that triggered the L1. The probability of a high amplitude L1 trigger increases with muon energy due to the increase of the photon yield from more energetic electro-magnetic showers.

3.6.2 Scanning

This section gives a summary of the scanning phase (section 3.4.1) of the reconstruction algorithm. Scanning over the angular space allows the selection to be applied to the hit sample. It also allows identification of some solutions as local rather than absolute χ^2 minima. Examples of several scans are shown in figures 3.10, 3.11 and 3.12. For each event, the number of hits that are found by the directional clustering algorithm and the negative logarithm of the χ^2 per degree of

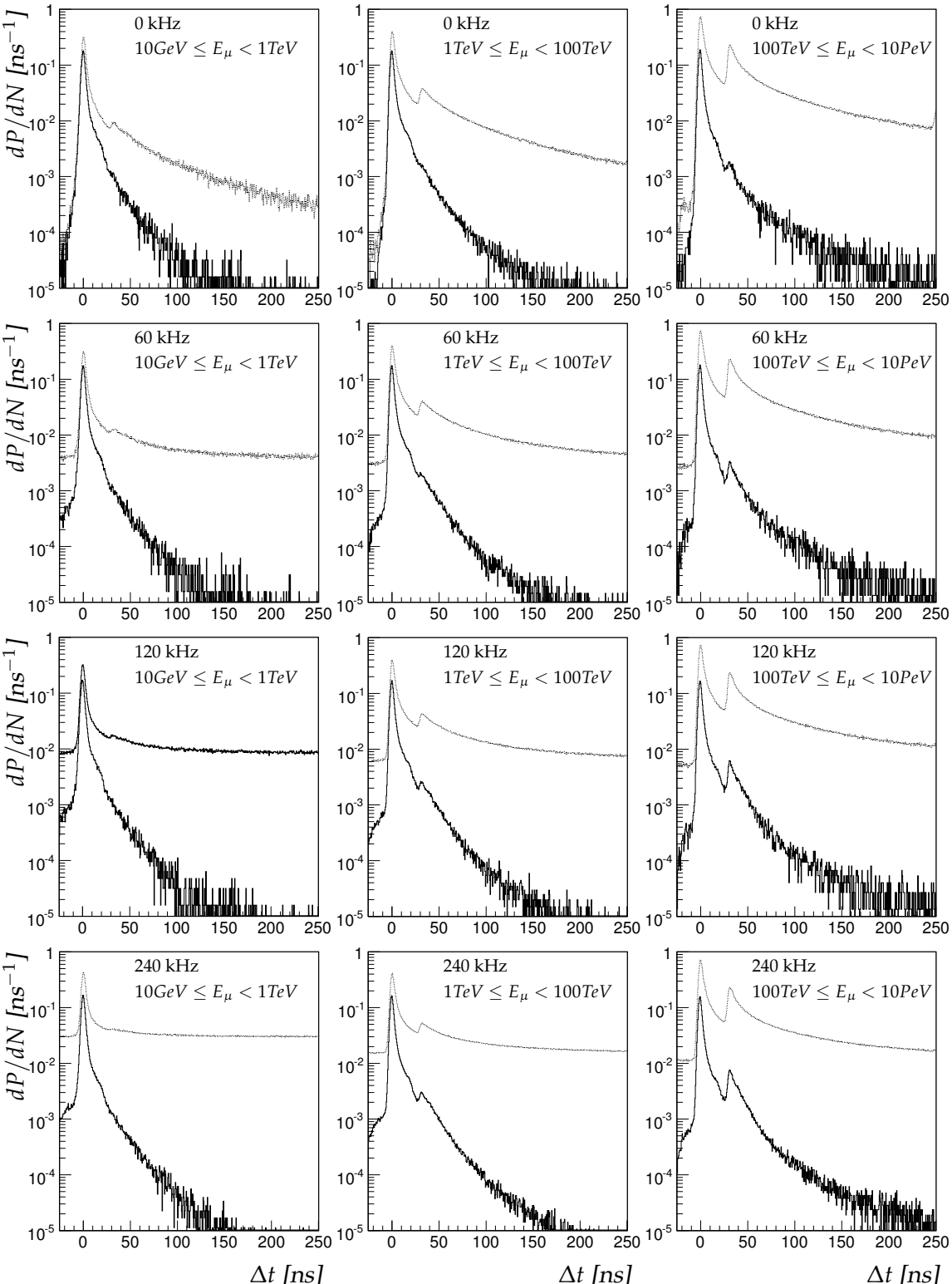

Figure 3.9: *Distributions of hit time residuals for different background rates and muon energy ranges. Each plot shows two lines, the top line is before hit selection, the bottom one is after hit selection.*

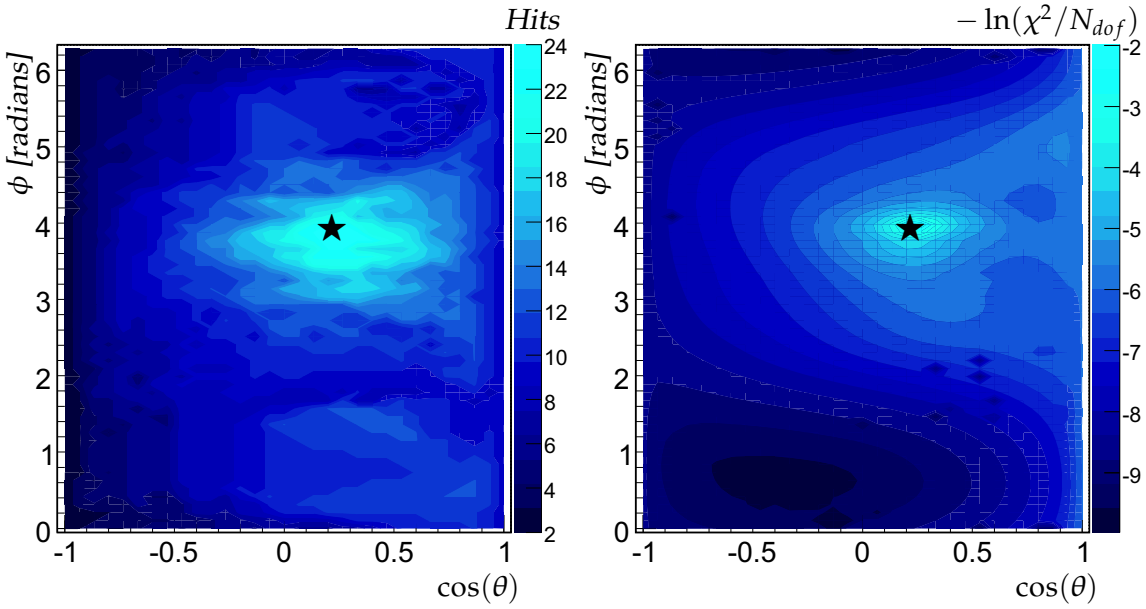

Figure 3.10: *Scan of the angular space for a 64 TeV muon. Left : number of associated hits. Right :* $-\ln(\chi^2/N_{dof})$*. The mark ★ : true track direction.*

freedom[1] is shown as a function of the direction. The χ^2 is obtained by making a fit with the angles fixed according to the given directions. The hits used in this fit are all the hits that caused the event to be triggered. The hit selection is omitted. In this way, the plots represent the landscape in which a χ^2 fitting procedure without hit selection should find a minimum. From figures 3.10, 3.11 and 3.12, some common observations can be made. The regions of the angular space in which the maximum number of hits could be found show a correlation with the true values of the track parameters. The existence of several disconnected local minima of the χ^2 values can be recognised.

It is expected that the direction in which the maximum number of hits (N_{max}) can be found using the hit selection procedure is close to the true muon direction. The angular residual between the true muon direction and the direction with N_{max} hits is shown in figure 3.13 as a function of scanning grid size ω/N_g (see section 3.4.1). If multiple solutions with N_{max} hits are found, the one with smallest residual is taken. It can be seen that the angular residual depends almost linearly on the grid size. The value for a scanning grid of 5 degrees is 5 degrees for an assumed background of 60 kHz. The actual resolution of the scanning phase is in general better than that due to the fact that the direction closest to the true direction can have a smaller number of associated hits.

[1]The negative logarithm of the χ^2 is taken to make the comparison with the contour plots. The logarithm reduces the dynamic range. The negation makes sure that a higher value corresponds to a 'better' χ^2.

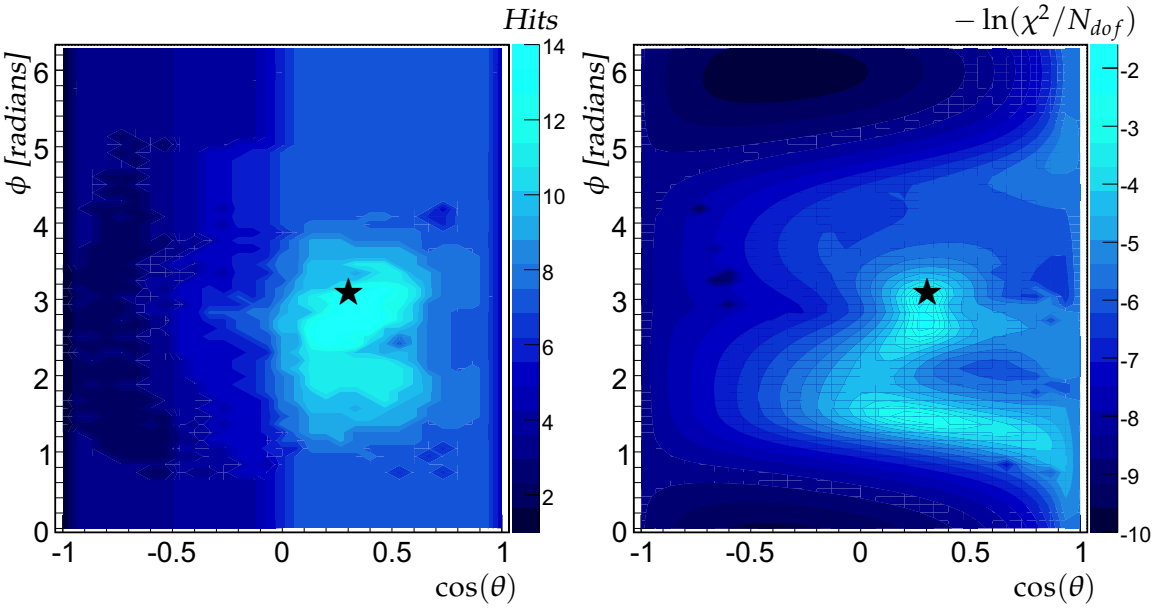

Figure 3.11: *Scan of the angular space for a 1.4 TeV muon. Left : number of associated hits. Right :* $-\ln(\chi^2/N_{dof})$*. The mark ★ : true track direction.*

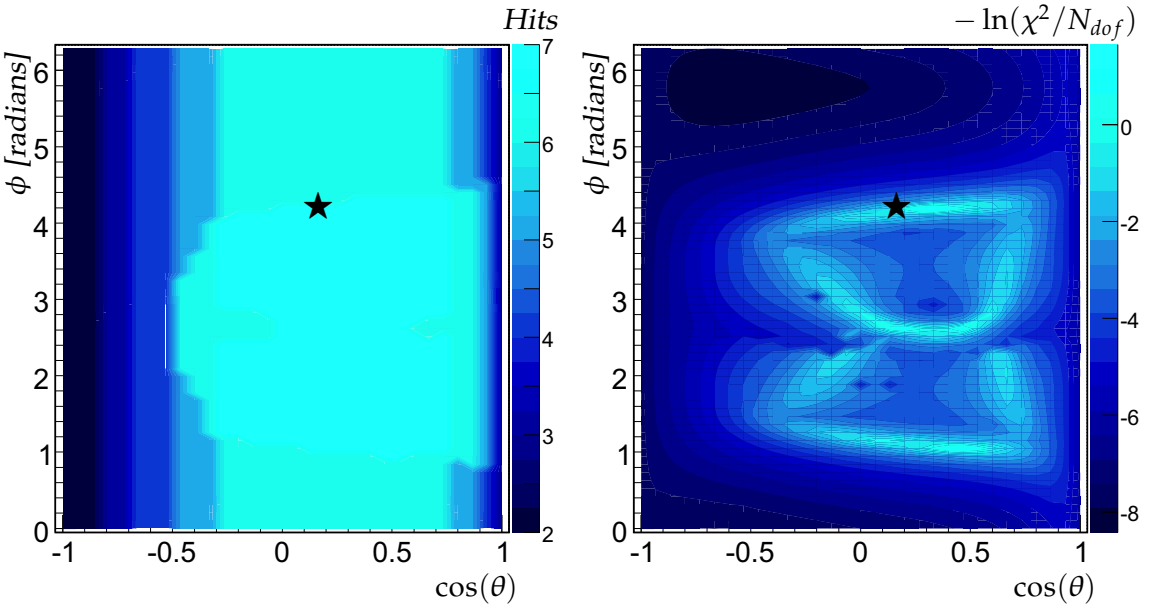

Figure 3.12: *Scan of the angular space for a 3 TeV muon. Left : number of associated hits. Right :* $-\ln(\chi^2/N_{dof})$*. The mark ★ : true track direction.*

The correlation between the number of associated hits and the probability of being close to the true direction can be used to speed up the further steps in the reconstruction. This can be done by excluding candidate directions with $N < (1 - P_{Ncut}) \times N_{max}$ hits from further steps (see section 3.4.2). The only parameter in this selection is P_{Ncut}, the fractional reduction of hits with respect to the maximum. The remaining fraction of candidate directions is shown in figure 3.14 for a grid size of 5 degrees at 60 kHz. The effect of this cut on the angular residual, calculated using the solution closest to the true direction, is also shown in figure 3.14. The value of P_{Ncut} used in this work is 0.2, which results in an average rejection of about 60% of the candidates while increasing the angular residual by about 10 %.

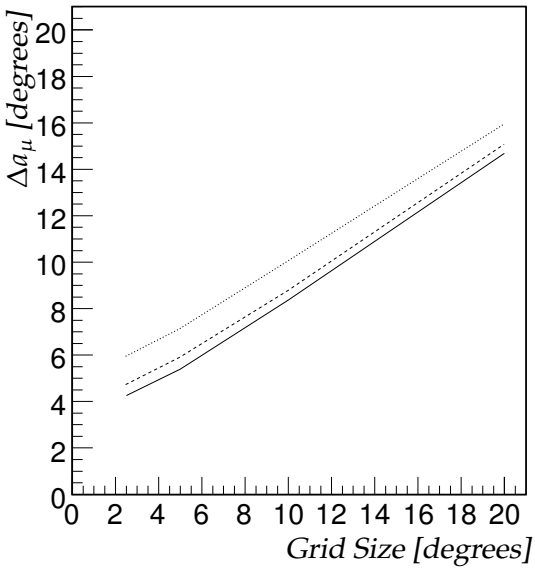

Figure 3.13: *Median of the angular residual Δa_μ as a function of the grid size used for scanning. The solid line corresponds to a random background of 60 kHz, the dashed line to 120 kHz and the dotted line to 240 kHz.*

3.6.3 χ^2 Fit

This section describes the χ^2 based fitting procedure. In this fit, the angles of the muon direction are added as additional free parameters.

Hit Removal

In the χ^2 fit, possible outliers can be removed iteratively, following a procedure described in section 3.4.2. The maximum allowed number of removed hits is defined a priori as a fraction of the total number of hits selected for the χ^2 fit and is referred to as f_r. The fraction of the number of fits with a χ^2 probability larger than 1 % has been studied as a function of the value of f_r. The χ^2 probability is calculated assuming a time resolution of $\sigma = 1.75$ ns for all hits. A hit is considered an outlier if $|\Delta t|/\sigma > 5$. This is done for a sample without background.

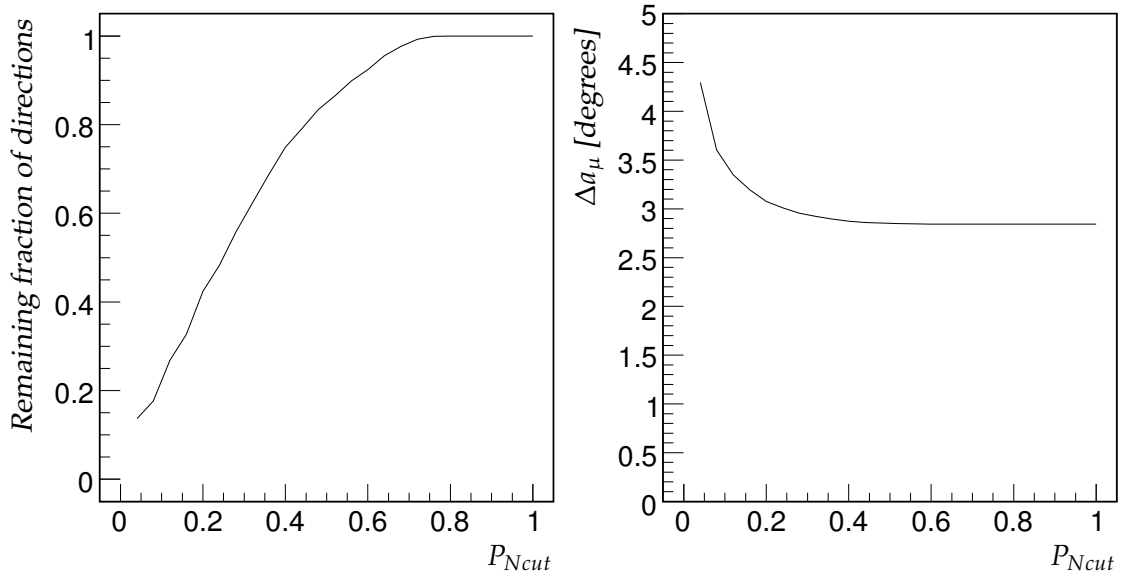

Figure 3.14: *Remaining fraction of candidate directions (left) and angular residual (right) as function of P_{Ncut}. P_{Ncut} is defined in the text..*

Figure 3.15 shows this relation. Allowing 10 % ($f_r = 0.1$) of hits to be removed increases the yield of the number of fits with a χ^2-probability larger than 1 % from about 40 % to 65 %. The value for f_r has been set to 0.2.

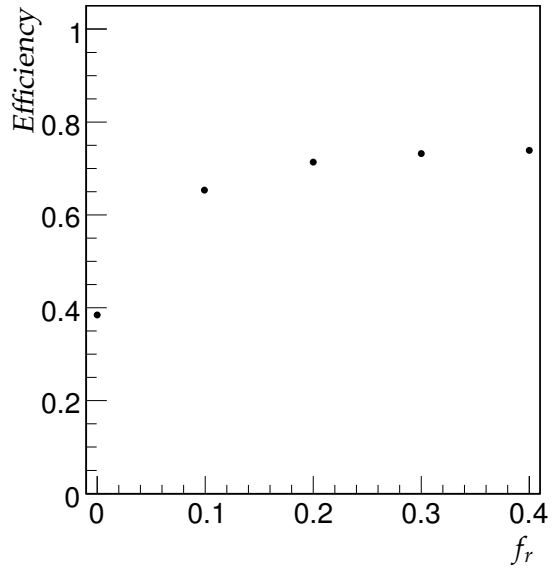

Figure 3.15: *Efficiency as function of the maximum fraction of hits allowed to be removed. The efficiency is defined as the fraction of events with a χ^2 probability $> 1\%$.*

Accuracy

The χ^2 fit includes all five track parameters in the optimisation process, including the angles which in the prefit were fixed. The error on the angle of the prefit passed on to the χ^2 fit can be controlled to some extent by the number of directions considered at the start. The probability of finding track parameters close to the true ones depends on the starting values. When there is a minimum of the χ^2 at the true parameter values, it is more likely to be found when the starting parameters are close to the true ones. How close the starting parameters have to be for a correct convergence has been investigated. The measure considered for this study is the angular residual. The χ^2 fit is started at different angles with respect to the true direction. The track is then rotated around the position of the track closest to the center of gravity of the hits. Figure 3.16 summarizes the results. As can be seen from figure 3.16, the angular residual is largest at low energies, especially below 100 GeV. This is due to the small number of hits that can be used for the reconstruction. Also, the angular residual tends to increase a bit at higher muon energies. This can be attributed to the contamination of hits in the tail of the time distributions. A cut in the χ^2 probability is expected to improve in the regions of high energy. At high rates (120 and 240 kHz) many of the fits which start close to the true values (0 and 1 degree) do not converge to the true direction. The high background rates clearly limit the angular resolution. In summary, the χ^2 fit typically improves the angular resolution from 2.5 degrees to 1 degree.

3.6.4 Full PDF Fit

Likelihood Values

In the full PDF fit, the estimators of the track parameters are those values which maximize the logarithm of the likelihood $\ln(L)$ (see section 3.1). The value of the likelihood at its maximum scales with the number of degrees of freedom involved. In order to account for this, the log-likelihood per degree of freedom, $\ln(L)/N_{dof}$ is used. This quantity is found to be effective in selecting good quality tracks as shown in reference [74].

The value of the likelihood at the true track parameters is referred to as L_{true}. If a maximisation of the likelihood is started at the true track parameters, then, in the limit of an infinite number of uncorrelated data points, it should find no better value than L_{true}. The convergence of the full PDF fit has been studied. This study was done for signal exclusively, no random background was added. The true track parameter values were taken as the start values of the likelihood maximisation. The value of the likelihood after the maximisation is referred to as L_{fit}. Figure 3.17 shows the distribution of $\ln(L_{fit})/N_{dof} - \ln(L_{true})/N_{dof}$. The contributions to the histogram from fits with different numbers of hits in the fit are indicated separately. It can be seen from figure 3.17 that in general the value of $\ln(L_{fit})/N_{dof} - \ln(L_{true})/N_{dof}$ is larger than the expected value of 0. This means

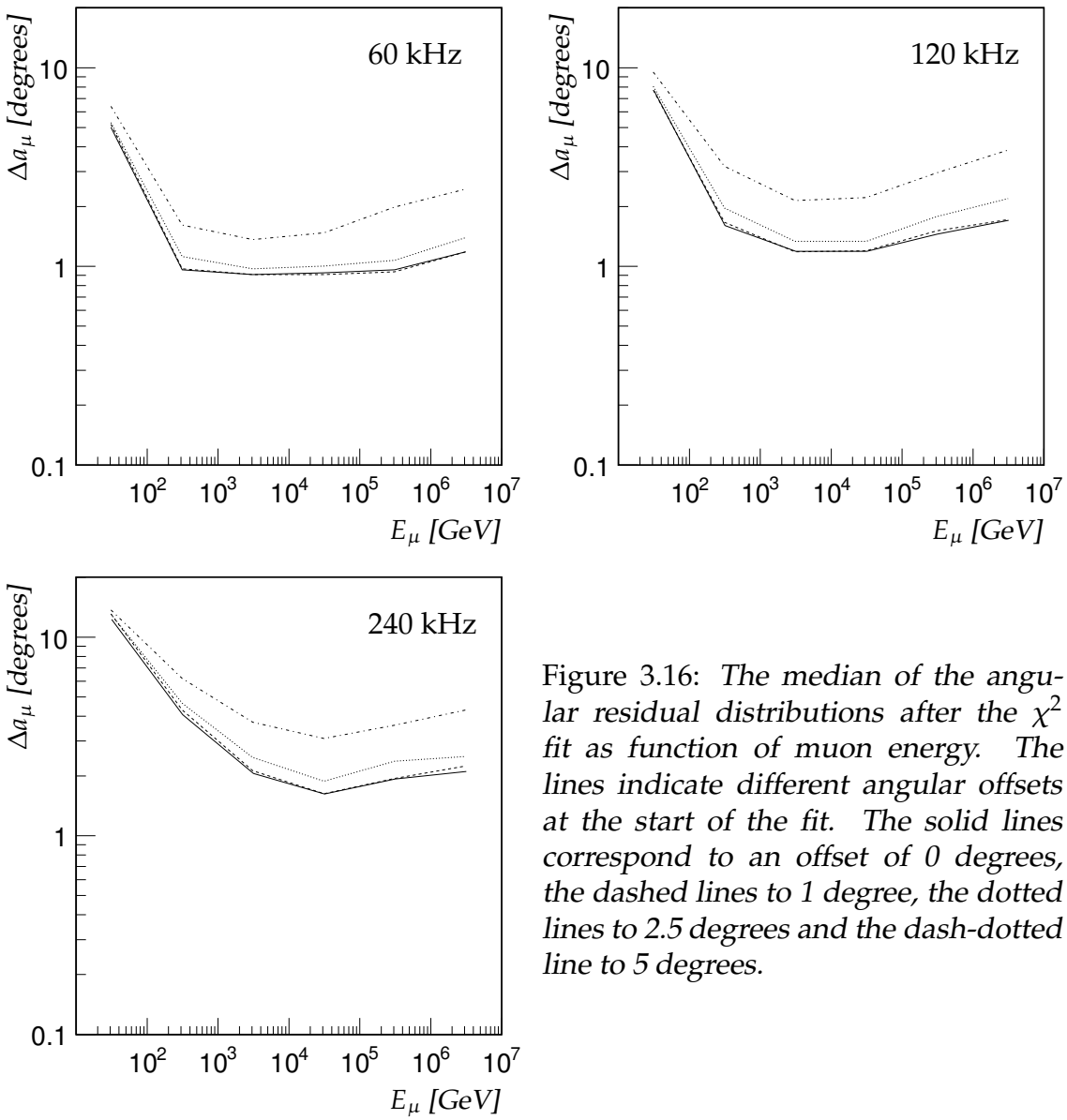

Figure 3.16: *The median of the angular residual distributions after the χ^2 fit as function of muon energy. The lines indicate different angular offsets at the start of the fit. The solid lines correspond to an offset of 0 degrees, the dashed lines to 1 degree, the dotted lines to 2.5 degrees and the dash-dotted line to 5 degrees.*

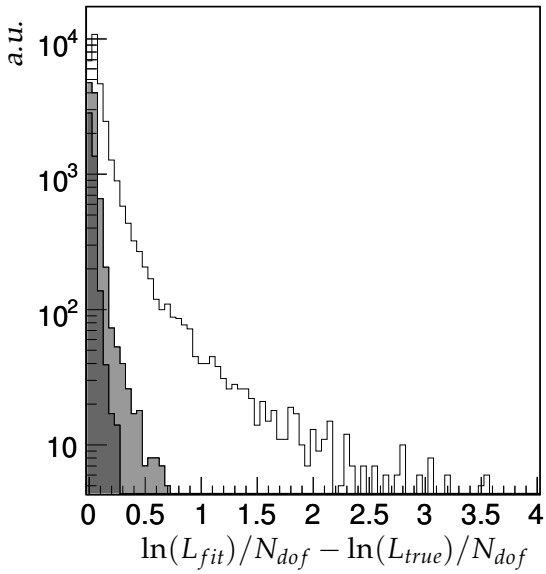

Figure 3.17: *Distribution of* $\ln(L_{fit})/N_{dof} - \ln(L_{true})/N_{dof}$. *The white distribution contains all events. The gray distribution contains events for which more than 75 hits were used to reconstruct the track. The dark gray distribution contains events in which more than 150 hits were used to reconstruct the track.*

that a maximum of the likelihood could be found that is larger than the truth. With an increasing number of hits used in the fit, the condition of infinite data is approached and the tail decreases. The extent of the tail is not solely determined by the statistical fluctuations at small numbers of hits. The larger values, $\ln(L_{fit})/N_{dof} - \ln(L_{true})/N_{dof} > 0.5$, are dominated by events which contain a set of correlated hits for which the measured time deviates from the expected time. Two distinct cases can be found. First are the events containing a large fraction of hits from an electro-magnetic shower occurring along the muon track. Figure 3.18 displays such an event. As can be seen in figure 3.18, a large fraction of the hits arrives later than the expected time. These hits are identified as originating from an electro-magnetic shower. The second case concerns events in which two muons cause a detectable signal in the detector. In figure 3.19, a simulated event is shown in which one muon originates from the charged-current neutrino interaction, and an other from a pion decay. The pion was created in the charged-current interaction.

The present PDF doesn't explicitly depend on the energy of the muon. It is clear though, that the hit time residual probability P^{sig} depends on the energy, as can be seen for example in figure 3.9. What can also be seen from this figure is that there is an interplay between the background and the contribution of the second ARS peak. At higher background rates, there is a higher probability that a signal hit ends up the second peak, because an earlier background hit caused the first ARS to make a hit. This relation is not taken into account, as the P^{sig} is modeled independently from the background rate. The modified P^{sig} as developed in this work describes the hit-time residual distribution better than the original, as can be seen from figure 3.4. A special feature is the decreased sensitivity to the correlated second ARS hits. The modified PDF is thus expected to perform better for a larger

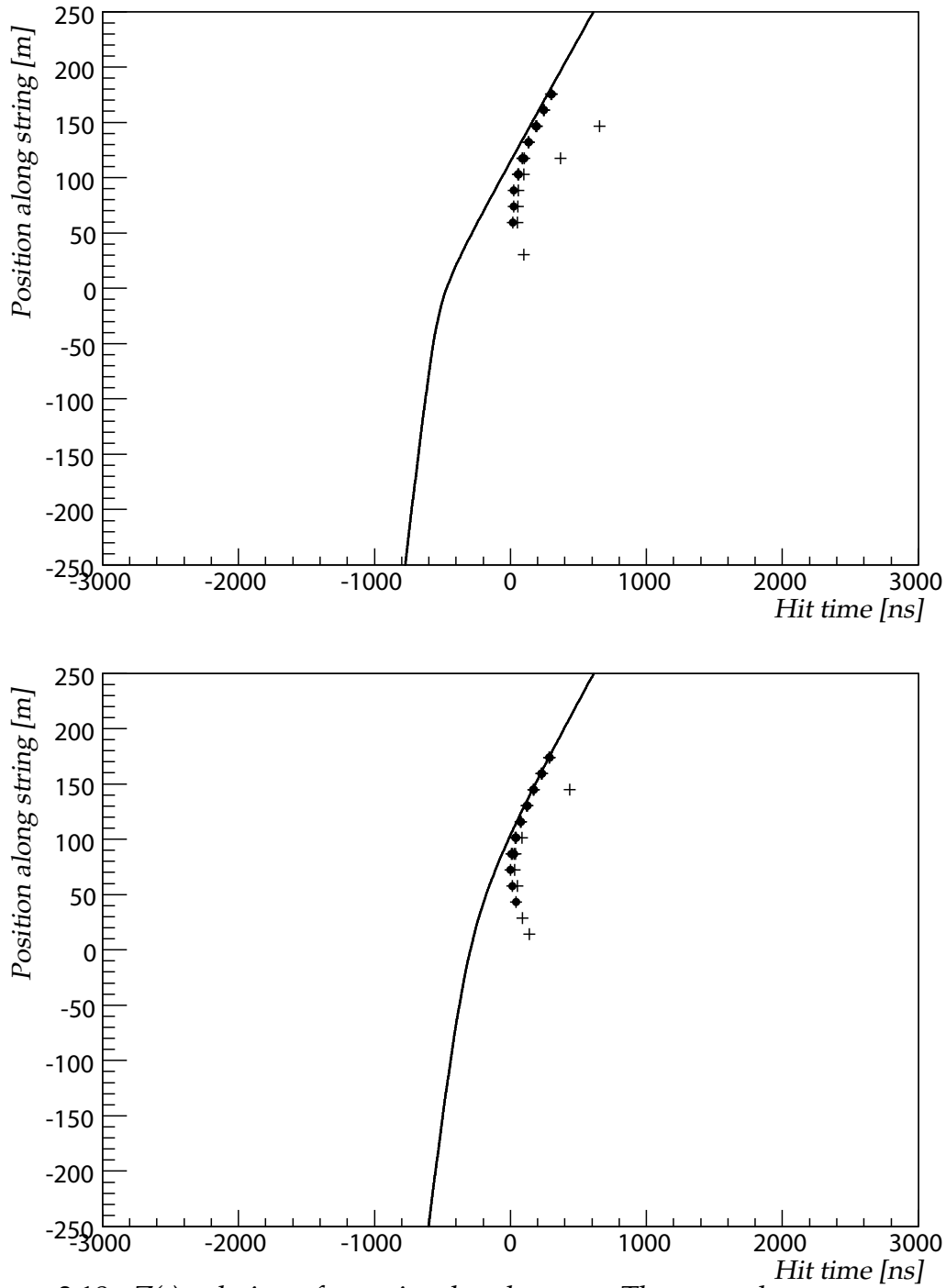

Figure 3.18: *Z(t) relations for a simulated event. The two plots correspond to different detector lines. The top plot corresponds to line 1 and the bottom to line 2 (see figure 2.8). The solid lines correspond to the expected arrival times of Cherenkov photons. The black dots and crosses are hits that originated from an electromagnetic shower occurring along the muon track. The black dots are the hits that caused the event to be triggered.*

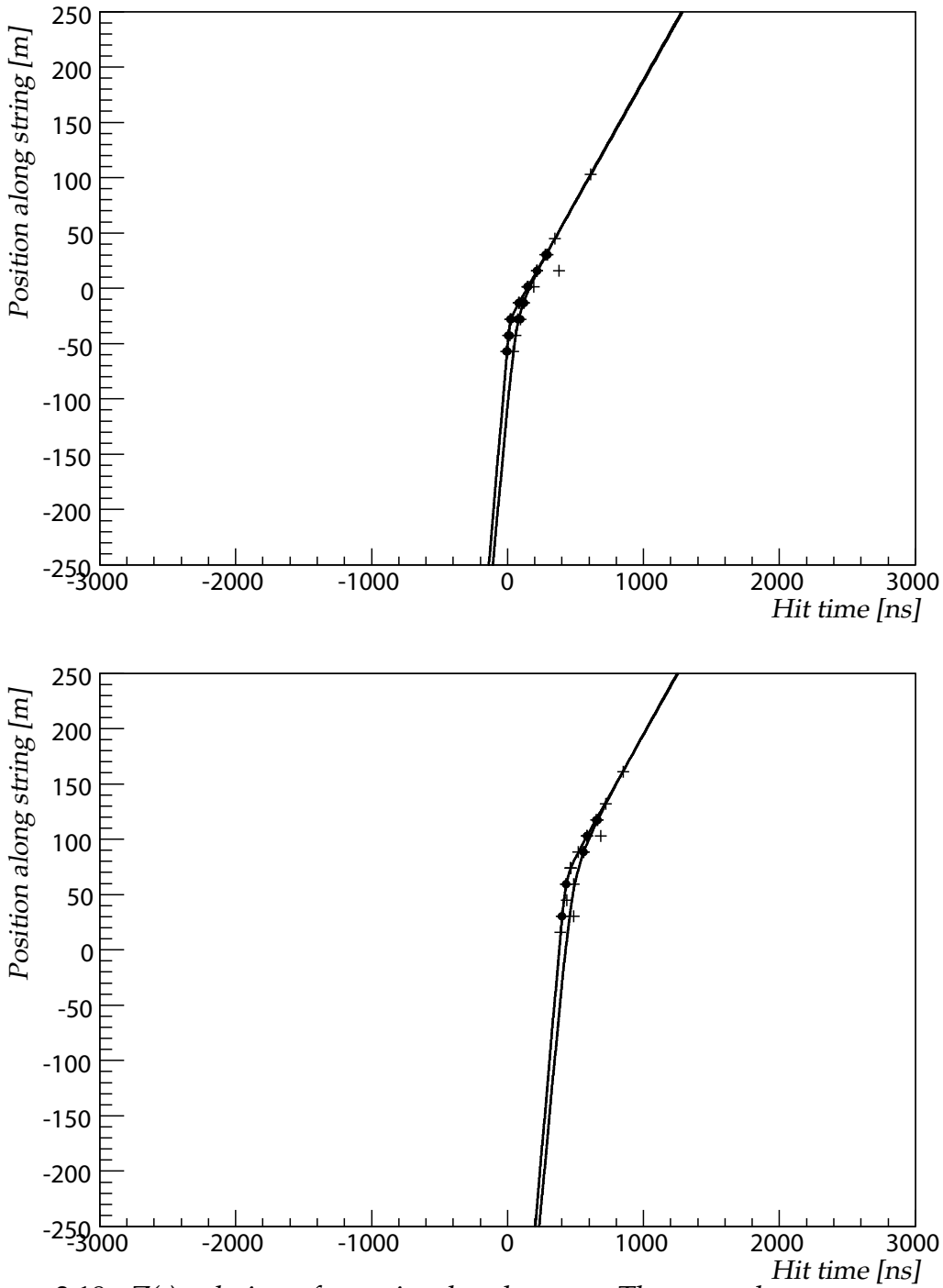

Figure 3.19: *Z(t) relations for a simulated event. The two plots correspond to different detector lines. The top plot corresponds to line 1 and the bottom to line 7 (see figure 2.8). The solid lines correspond to the expected arrival times of Cherenkov photons. In this event an additional muon originating from pion decay can be identified (the rightmost line). The black dots and crosses are hits caused by either line.*

range of muon energies.

A study of $\ln(L)/N_{dof}$ as a function of energy and background rate has been made. Figure 3.20 shows for three different background rates, the distribution of $\ln(L)/N_{dof}$ as a function the muon energy. The likelihood values are calculated with the fit starting at the true track coordinates. For all background rates a dependence on the energy can be seen. The original PDF shows a change of slope with increasing energy. This indicates a deviation from the expected trend that the likelihood increases with energy as the signal-to-noise of the hits increases. This is due to an increasing contribution of the second ARS hits. The modified PDF shows a more monotonous behavior. It can be concluded that the modification of the PDF and the associated hit selection lead to a better compatibility between the PDF and data.

Accuracy

The convergence of the full PDF fit is evaluated in the same way as the χ^2 fit in the previous section. Figure 3.21 summarizes the resolution after the fit as function of background rate and muon energy. It can be seen from figure 3.21 that the full PDF fit converges to smaller angular residuals than the χ^2 fit (compare figure 3.16). For small values of the angular offset, the value of the angular residual after the fit is consistently well below 1 degree and for higher energies well below 0.4 degrees.

3.6.5 Complete Algorithm

In this section the performance of the complete algorithm will be discussed. This is done by presenting the results after each stage of the fit. The results after the χ^2 stage will be presented first and then the results of the full PDF fit.

One feature of the algorithm was not taken into account so far when evaluating the different stages, especially the χ^2 and full PDF stage: the scanning of angular space not only maps out local minima, but can also provide different paths to a possibly broad (global) minimum. This can lead to multiple solutions which are (almost) identical. Solutions are considered identical when they differ less than 1 degree. When such a set of solutions is found, the different solutions are sorted according to the number of associated hits. The solution with the largest number of hits is taken as the best solution, and if there are different solutions with equal numbers of hits, the solution with the smallest χ^2 or the largest likelihood is selected.

χ^2 fit

As the algorithm, in general, produces several different solutions, various ways of selecting the 'best' solution are presented. The solutions are sorted based on

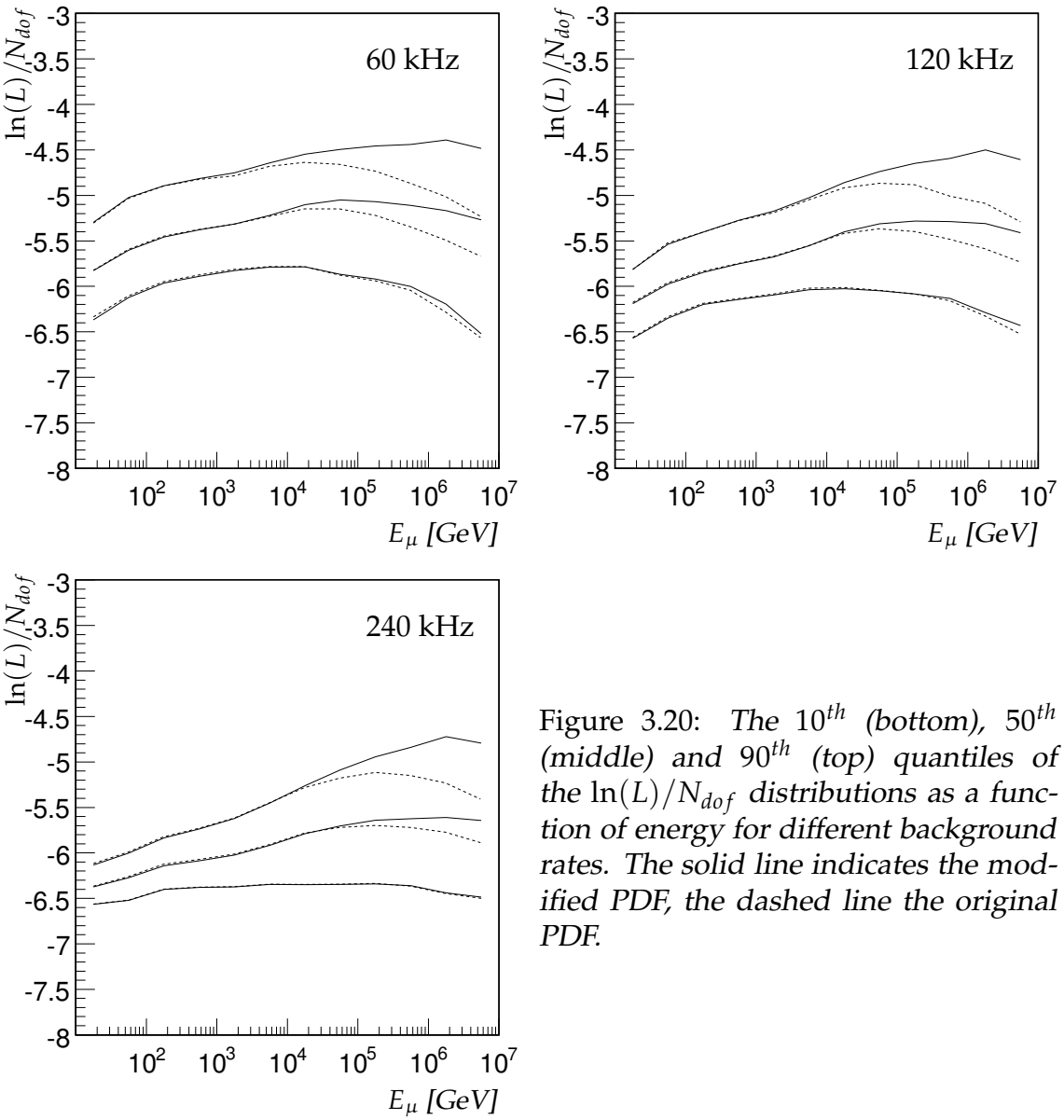

Figure 3.20: *The 10^{th} (bottom), 50^{th} (middle) and 90^{th} (top) quantiles of the $\ln(L)/N_{dof}$ distributions as a function of energy for different background rates. The solid line indicates the modified PDF, the dashed line the original PDF.*

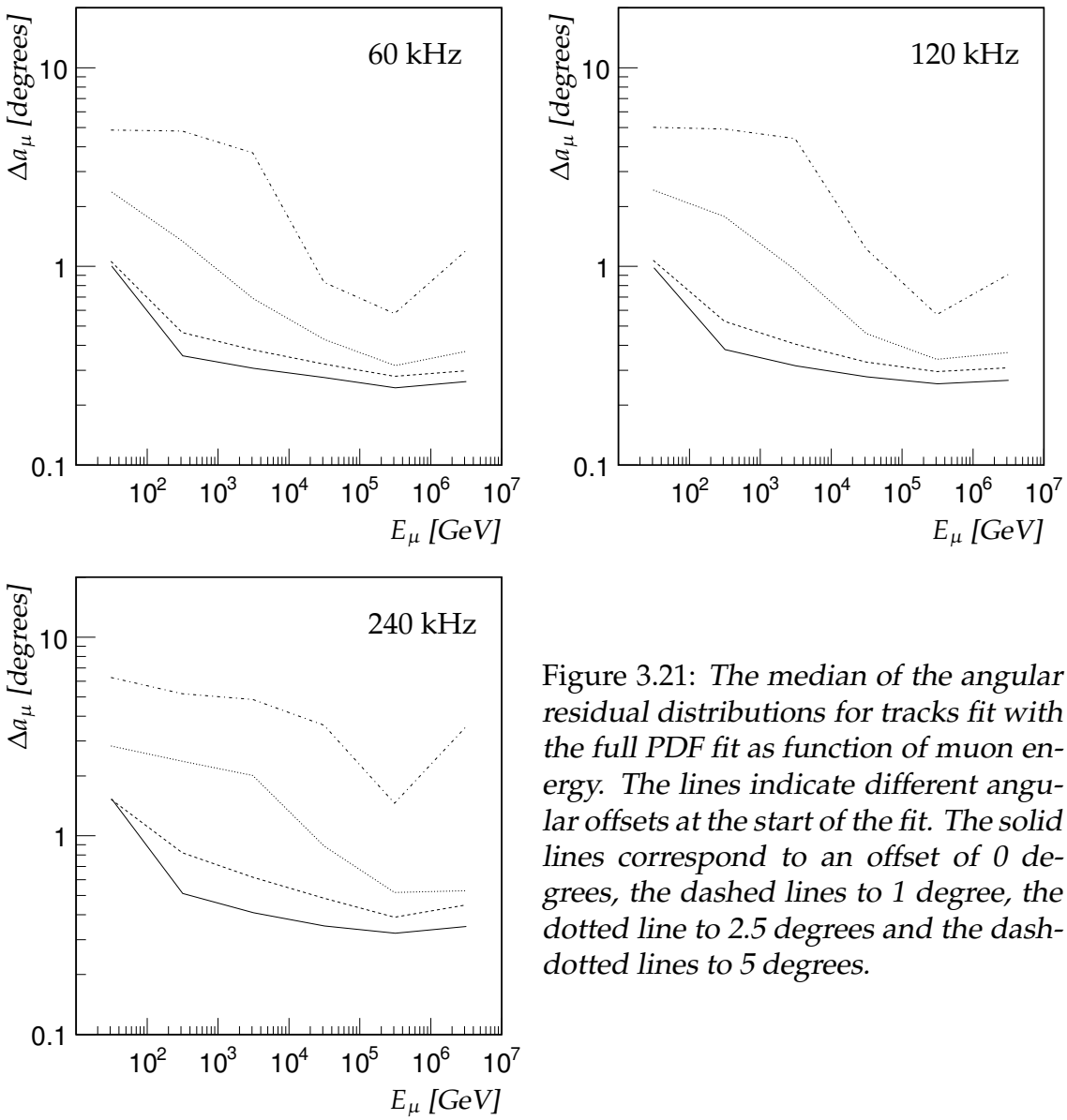

Figure 3.21: *The median of the angular residual distributions for tracks fit with the full PDF fit as function of muon energy. The lines indicate different angular offsets at the start of the fit. The solid lines correspond to an offset of 0 degrees, the dashed lines to 1 degree, the dotted line to 2.5 degrees and the dash-dotted lines to 5 degrees.*

the number of hits and on the χ^2 likelihood. The solution with the largest number of hits is taken as the best solution. If there are different solutions with the same number of hits, the solution with the smallest χ^2 is taken. Optionally, only solutions with a χ^2 probability of 1 % or larger are considered.

Figure 3.22 shows the χ^2 probability distribution after the fit. The value of the assumed time resolution is set to 1.75 ns for all hits. This is the same value used in the hit-removal. The distribution is reasonably flat indicating a good agreement between model and data. The rise towards higher values of $P(\chi^2)$ indicates a slight overestimate of the assumed time resolution. The peak at zero contains events with a large fraction of outlier hits. The resulting hit-time residual distribution is shown in figure 3.23, together with a fit of a Gaussian distribution. Only hits that are used for the reconstruction are included. The width of the fitted distribution is about 2 ns.

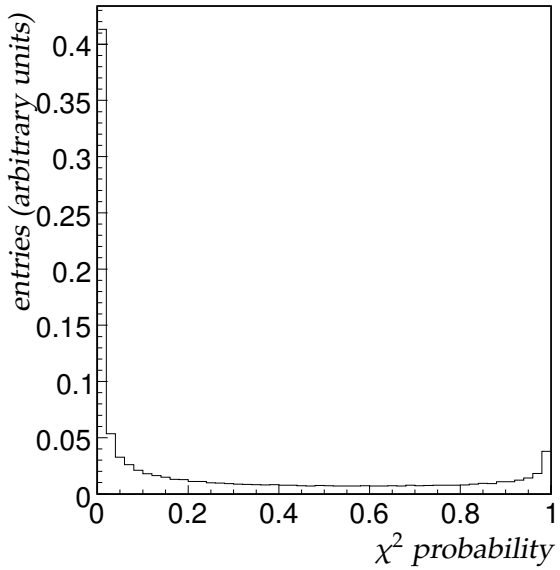

Figure 3.22: *Distribution of the χ^2 probability after the χ^2 fit. A grid size of 5 degrees is used and a background rate of 60 kHz has been assumed.*

The resolution of the χ^2 fit is summarized in figure 3.24 for an angular grid with a step size of 5 degrees. By comparing the lines corresponding to the median in figure 3.24 to those in figure 3.16, it can be seen that the angular residual has improved. For low rates the selection criterium is capable of selecting the solution closest to the true direction. The selection of fits based on χ^2 probability larger than 1 % is effective in decreasing the angular residual of the remaining events, especially at higher rates. The same sorting criterium is less effective for larger angular residuals. Although the angular resolution is the most important parameter for astrophysics, the error on the position of the muon has also been studied. In the context of the algorithm, a good estimate of the position helps in the next step of the fitting procedure. The next step is in this case the full PDF fit. The error on the position is measured by the distance of closest approach between the true muon track and the reconstructed track. As with the angular residuals this quantity is summarized as function of energy for the different background

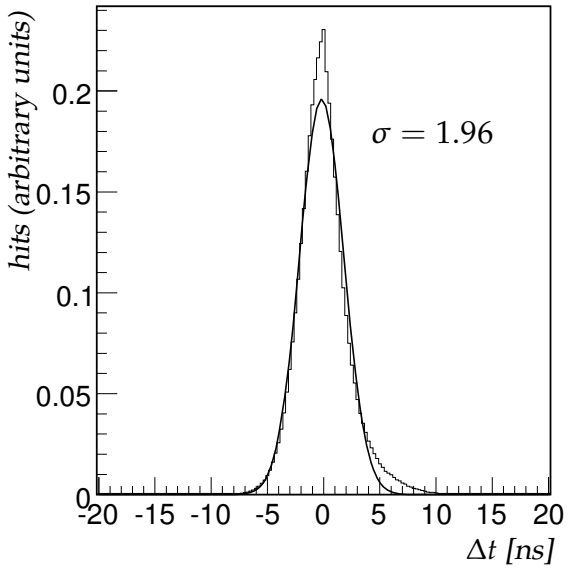

Figure 3.23: *Distribution of the hit time residuals after the χ^2 fit. A grid size of 5 degrees is used and a background rate of 60 kHz has been assumed. The smooth curve is a fit of a Gaussian distribution to the data (see text).*

rates. The result is shown in figure 3.25. As with the angular residual, the error on the position increases with the background rate, the median reaches 2 meters at high rates. There is a larger difference between the results using the best solution and the selected one. This is to be expected as the best solution is defined in terms of angular resolution, and the χ^2 probability cut selects on the overall quality.

Full PDF fit

The accuracy of the fit after the full PDF fit will now be presented. As after the χ^2 stage, there are in general multiple track candidates due to the angular scanning in the algorithm. In section 3.6.4 the likelihood per degree of freedom was introduced. This quantity is used to sort the different solutions for a given event. The solution with the largest likelihood per degree of freedom is taken as the preferred solution. In figure 3.26 the angular residuals are shown as a function of energy for different background rates. As can be seen from figure 3.26 the lines corresponding to the selected solution and the ideal case overlap for small angular residuals, except at the lowest energies. This validates the likelihood per degree of freedom as a sorting criterium. The angular residual (median) drops below 1 degree for about 100 GeV muons at 60 kHz, for 300 GeV muons at 120 kHz and 240 kHz. The angular residual (median) reaches 0.3 degrees for about 30 TeV muons at 60 kHz. At 120 and 240 kHz this angular resolution is reached at about 200 TeV.

The likelihood per degree of freedom is used to select the preferred solution. It is also a measure of fit quality. This was shown for instance in reference [74]. There, a cut on the likelihood per degree of freedom was used to separate well reconstructed tracks from poorly reconstructed tracks. The two most important

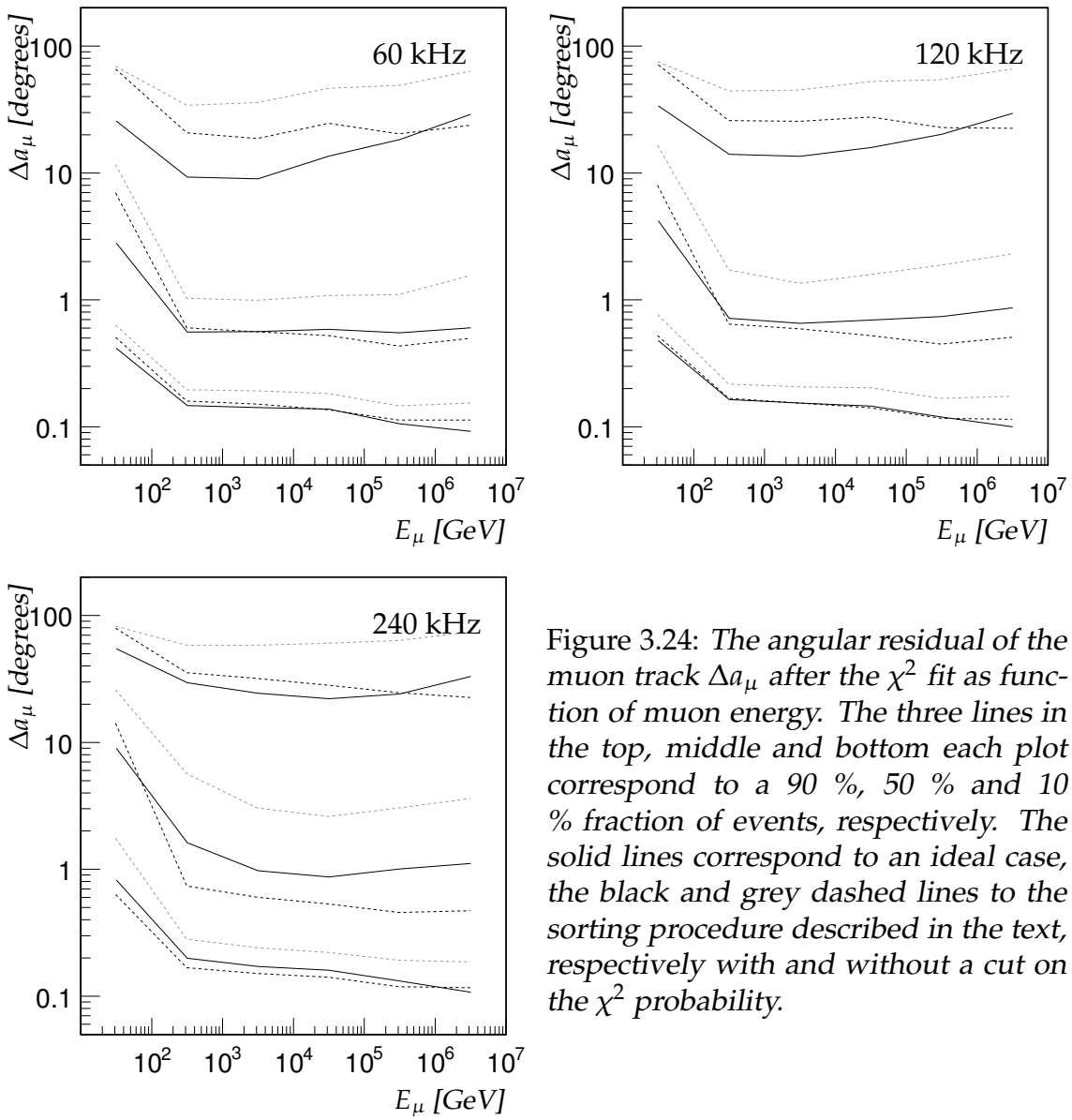

Figure 3.24: *The angular residual of the muon track Δa_μ after the χ^2 fit as function of muon energy. The three lines in the top, middle and bottom each plot correspond to a 90 %, 50 % and 10 % fraction of events, respectively. The solid lines correspond to an ideal case, the black and grey dashed lines to the sorting procedure described in the text, respectively with and without a cut on the χ^2 probability.*

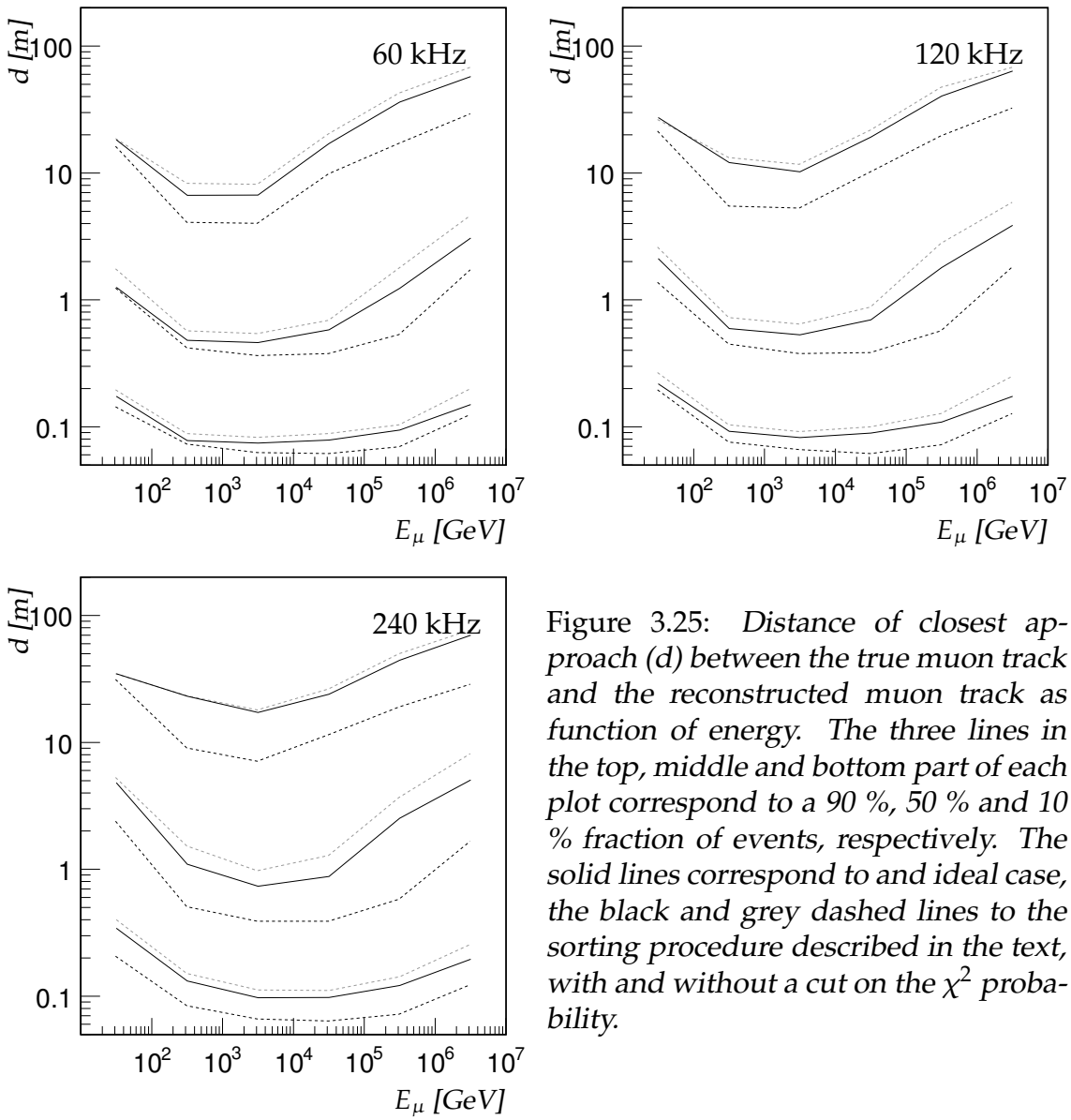

Figure 3.25: *Distance of closest approach (d) between the true muon track and the reconstructed muon track as function of energy. The three lines in the top, middle and bottom part of each plot correspond to a 90 %, 50 % and 10 % fraction of events, respectively. The solid lines correspond to and ideal case, the black and grey dashed lines to the sorting procedure described in the text, with and without a cut on the χ^2 probability.*

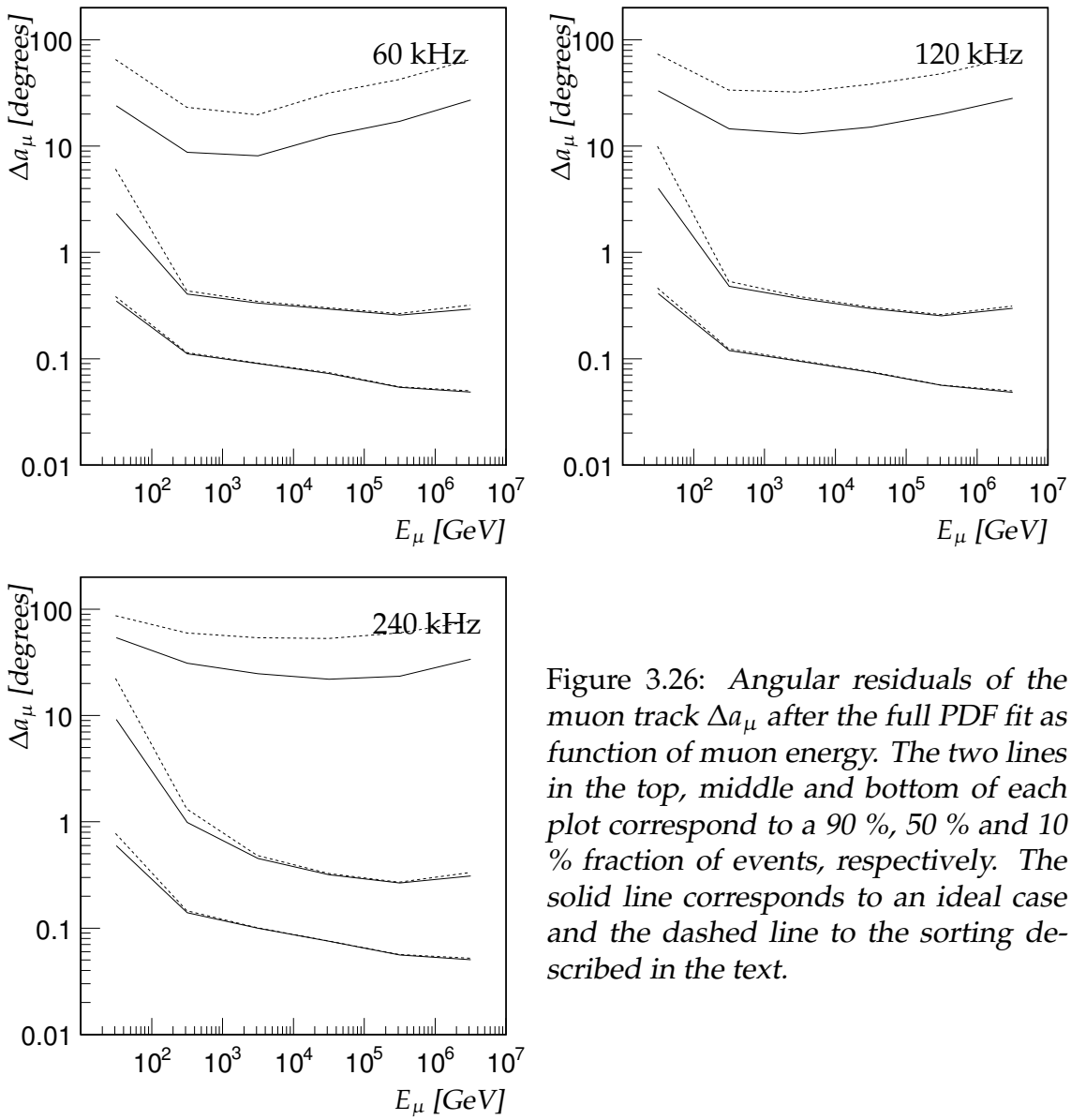

Figure 3.26: *Angular residuals of the muon track Δa_μ after the full PDF fit as function of muon energy. The two lines in the top, middle and bottom of each plot correspond to a 90 %, 50 % and 10 % fraction of events, respectively. The solid line corresponds to an ideal case and the dashed line to the sorting described in the text.*

features related to a cut on the likelihood per degree of freedom will be discussed. First, as shown in section 3.6.4, the behavior of the likelihood per degree of freedom depends on the background rate. Thus a cut on this quantity behaves differently for different background rates. The optimum value will be different for different background conditions. Which brings us to the second point. In general, a cut to improve quality has negative consequences for the efficiency. The fit quality, or accuracy, and efficiency are two related quantities. The relation between these two quantities has been studied in more detail. The event samples for the different background rates were divided in three energy bins. The first with 1 GeV $< E_\mu \leq$ 1 TeV, the second with 1 TeV $\leq E_\mu <$ 100 TeV and the third with 100 TeV$\leq E_\mu <$ 10 PeV, referred to as low, medium or high energies, respectively. To each of these samples, different cuts on the likelihood per degree of freedom were applied. For each of these cut values, the median of the angular residual distribution was calculated, together with the efficiency. The efficiency is defined as the remaining fraction of events with respect to all reconstructed events. The results are shown in figure 3.27. As can be seen from figure 3.27 the efficiency decreases with increasing cut values, while the accuracy increases. As seen before, the accuracy of the fit increases with energy. It can also be seen that, with increasing background rates, the cut levels for a given efficiency and accuracy increase. This reflects the overall shift of the likelihood per degree of freedom distribution as shown in section 3.6.4. Another observation is that for different background levels, the accuracies for a given efficiency differ by a small amount, typically less than 15 %.

3.6.6 Error estimates

The pull of a fitted quantity is defined as the difference between the fitted quantity and the true quantity (the residual) divided by the estimated uncertainty (one sigma error). Thus for the zenith angle θ the pull is $\left(\hat{\theta} - \theta\right) / \sigma_{\hat{\theta}}$. Ideally, the distribution of the pull should be a Gaussian distribution with mean 0 and width 1. For a maximum likelihood fit, generally, the 1σ limit is given by the parameter values for which $\ln(L_{max}) - \ln(L) = 0.5$ with L_{max} the maximum likelihood value resulting from the fit. In the limit of infinite data, the distributions can be described by a Gaussian function. In this case, the error matrix $\mathbf{V}$ is given by the inverse of the second derivative, or Hesse, matrix $\mathbf{H}$:

$$\mathbf{V} = \mathbf{H}^{-1} \tag{3.23}$$

$$\mathbf{H}_{ij} = \frac{-\partial^2 \ln L}{\partial x_i \partial x_j}\Big|_{L=L_{max}} \tag{3.24}$$

where $\vec{x} = (\theta, \phi, a, b, t_0)$ is the vector of track parameters. The Hesse matrix is calculated during the fit procedure and is determined together with the estimated

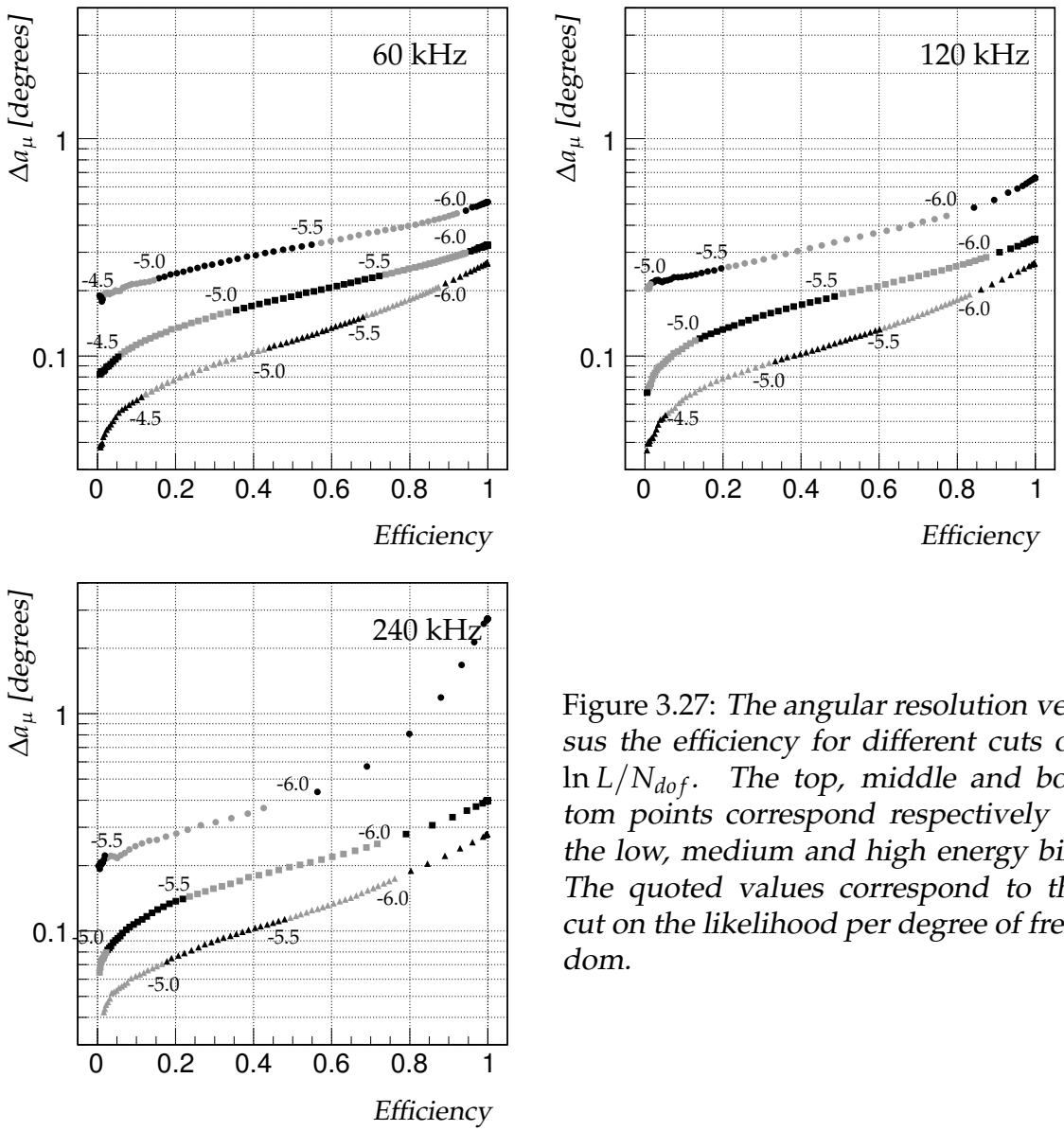

Figure 3.27: *The angular resolution versus the efficiency for different cuts on* $\ln L/N_{dof}$. *The top, middle and bottom points correspond respectively to the low, medium and high energy bin. The quoted values correspond to the cut on the likelihood per degree of freedom.*

track parameters. The diagonal elements of $\mathbf{V}$ are the variances of the track parameters, $(\sigma^2_{\hat{\theta}}, \sigma^2_{\hat{\phi}}, \sigma^2_{\hat{a}}, \sigma^2_{\hat{b}}, \sigma^2_{\hat{t}_0})$ and are used to calculate the pull values. The distributions are shown in figure 3.28 for the zenith angle and the azimuthal angle. The pull distributions in figure 3.28 have a similar shape. As expected, they peak at zero. The distributions are not fully Gaussian as they have longer tails towards negative and positive values. These tails are due to events in which either a local minimum of the likelihood was found or the global minimum did not correspond to the true muon direction. This leads to an underestimation of the error. A Gaussian function has been fitted to the data in the interval $-3 \leq \text{pull} \leq 3$. This includes more than 75 percent of the data. The widths of the fitted functions are indicated in figure 3.28. The fitted widths are typically 1.2. This indicates a consistent description of the PDF. The fitted widths are in reasonable agreement with the expected value of 1, but the errors are slightly (20%) underestimated.

3.6.7 Track length

A muon track is measured across a certain longitudinal distance. When the muon energy exceeds 100 GeV, it can traverse the complete detector. One expects that the accuracy with which the track parameters can be determined, depends to certain extent on the length of the track that is sampled. In order to estimate this effect, the quantity $\Delta z^{'}$ is used. This quantity is equal to the largest distance between two hits, measured along the track. So, in the reference frame defined by the track direction (see section 3.2) $\Delta z^{'}$ equals the difference between the hits with the largest and smallest z coordinate :

$$\Delta z^{'} = z^{'}_{max} - z^{'}_{min} \tag{3.25}$$

The collection of hits used by the full PDF fit includes hits caused by the random background. When calculating $\Delta z^{'}$ these background hits should be avoided. For this reason, only the hits selected by the 1D clustering algorithm (see section 3.3.1) are considered when calculating $\Delta z^{'}$. The relation between the median of the angular residual of the muon Δa_μ and $\Delta z^{'}$ is shown in figure 3.29 for different background rates. The assumed neutrino energy spectrum is proportional to E^{-2}. Figure 3.29 shows a strong dependence of the muon angular residual on the sampled track length. With a sampled track length of about 150 meters and more, the angular residual drops below 1 degree. For a background rate of 240 kHz this happens at 180 meters. At 380 meter track length, the median angular residual reaches 0.1 degree for a random background rate of 60 kHz. The slope of the curve at the end of the plot, which is limited by the detector geometry is still negative, indicating that a larger detector would improve the angular residual even more. The right plot of figure 3.29 shows a box plot of the angular residual versus the sampled length. The size of the boxes indicates the relative occurrence of a certain track length and angular residual. It can be seen that most of the tracks

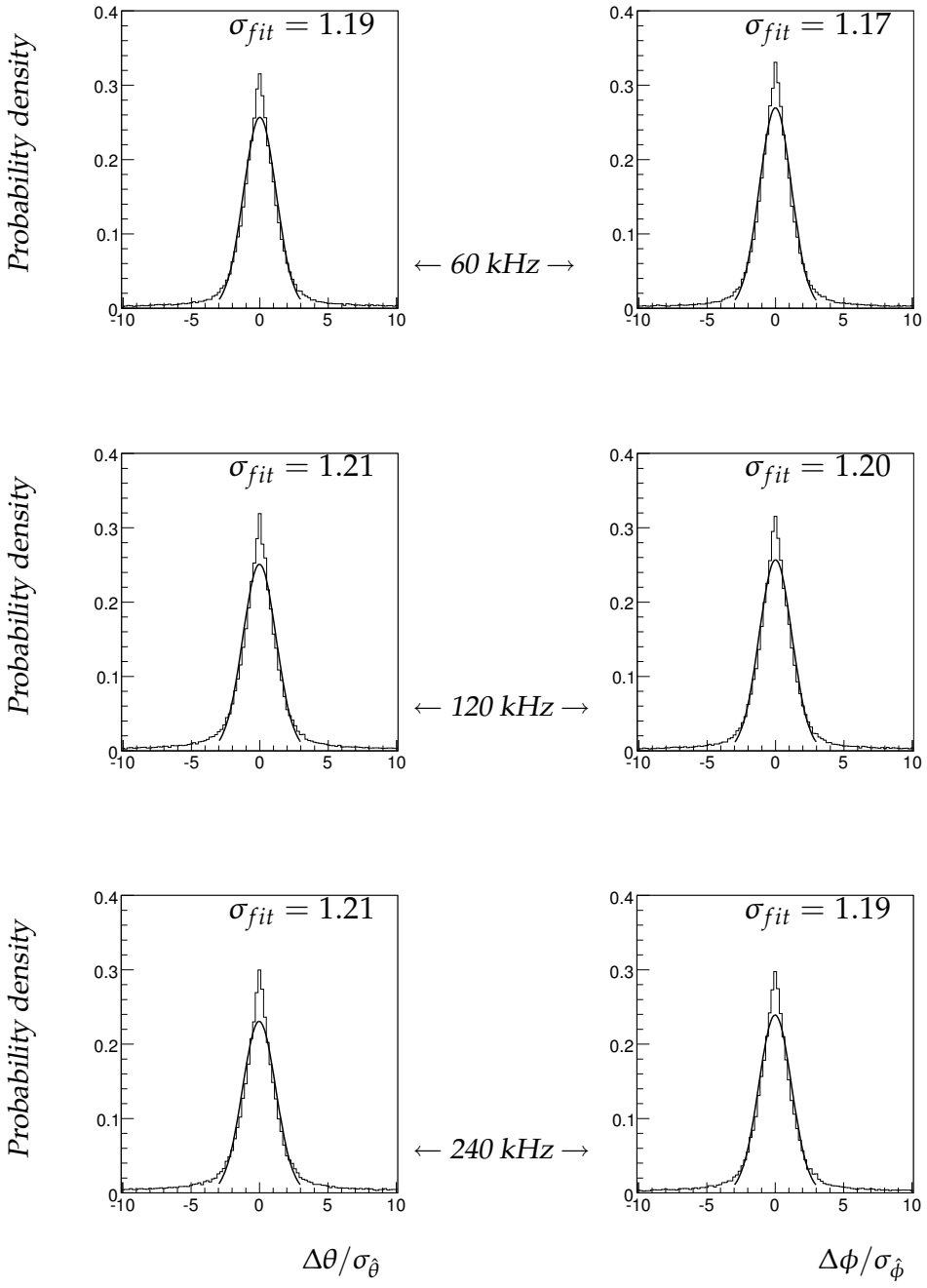

Figure 3.28: *Pull distributions for the zenith (left) and azimuth (right) angles. The distributions are shown for different random background rates.*

have a sampled length around 200 meters, which is characteristic for the Antares neutrino telescope.

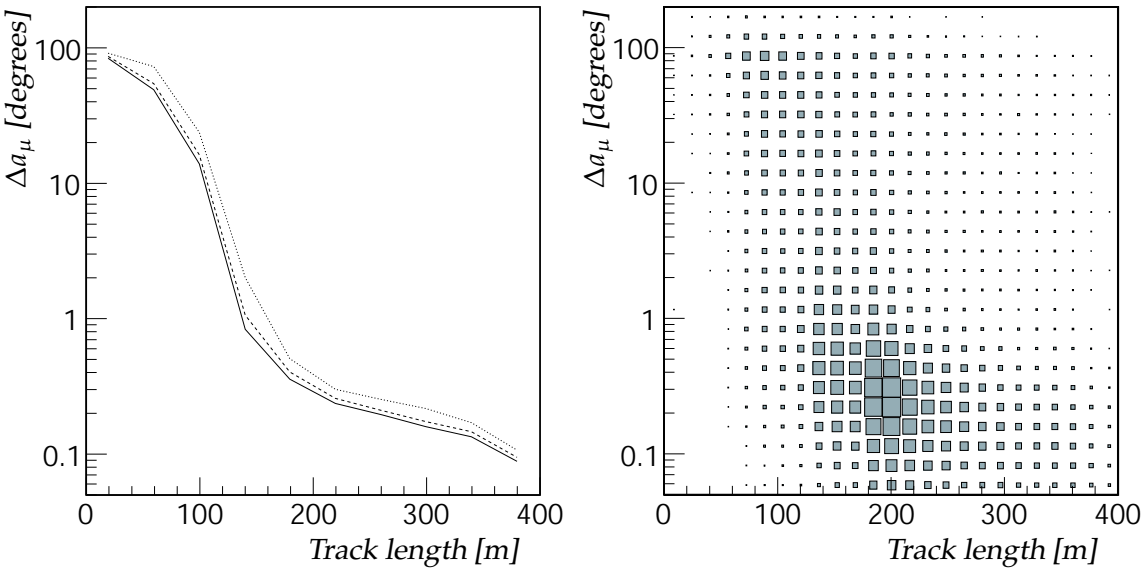

Figure 3.29: *Left : The median angular residual after the full PDF fit as function of estimated track length in the detector. The line types indicate different background rates. The solid line corresponds to 60 kHz, the dashed line to 120 kHz and the dotted line to 240 kHz. Right : Scatter plot of angular residual versus the estimated track length in the detector.*

3.6.8 Compatible solutions

The muon track reconstruction procedure starts out with a scan of the angular space to map out all solutions. In the consecutive fitting steps, the angles are free parameters. If a track is not rejected on basis of the number of selected hits, it can converge to a local optimum. Track candidates with different starting angles can converge to the same local or global minimum of the χ^2 or likelihood. When the global minimum is well defined it is more likely that several track candidates will converge to this same minimum. So, the number of track candidates that converge to the same solution can be considered as a measure for the overall quality. As explained before, tracks that converge to within 1 degree are collected and the one with the largest number of associated hits is taken. This is done for the χ^2 fitting step and for the full PDF fitting step. The number of converged tracks for a given solution are propagated from the χ^2 step on to the full PDF fit, and are taken into account when calculating the final number of track candidates that converged to a certain solution. This number is referred to as N_{comp}. This quan-

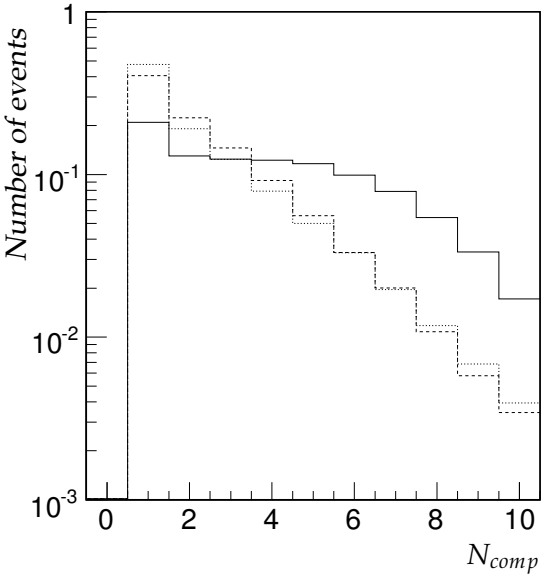

Figure 3.30: *Distribution of the number of compatible solutions N_{comp} after the full PDF fit. The solid line indicates a random background of 60 kHz, the dashed 120 kHz and the dotted 240 kHz.*

tity is already to some extent present in the fitting procedure developed in [74]. Now it is defined in a more rigorous way. Figure 3.30 shows the distribution of N_{comp} for the solution with the largest likelihood per degree of freedom after the full PDF fit for different rates. It can be seen from figure 3.30 that all distributions are peaked at one. A tail containing events in which multiple track candidates converged to the same solution is present. The size of this tail decreases with increasing random background rate. This can be expected as the minimum of the negative likelihood becomes less pronounced. The muon angular residual as function of N_{comp} is shown in figure 3.31. It can be seen from figure 3.31 that the events reconstructed with an angular residual smaller than 1 degree are dominated by events with $N_{comp} > 1$. It can also be seen that with increasing random background rates, the solutions with $N_{comp} > 1$ migrate to lower values of N_{comp} and to larger angular residuals. To conclude, the value of N_{comp} can be used as an indicator of track quality.

3.7 Summary

The muon track reconstruction algorithm presented in this chapter consists of several elements. It includes a partial scan over the phase space to map out local solutions. This scan is combined with a hit selection procedure which aims to maximize the purity of the hits with respect to the assumed muon. Candidate tracks from the scanning phase are used to start a final fit χ^2 based fit using the selected hits. This method aims at maximizing the performance without relying on detailed knowledge of the environmental properties. This robustness makes it particular useful at the beginning of detector operation. The performance of the reconstruction was evaluated and shown to able to achieve a resolution of

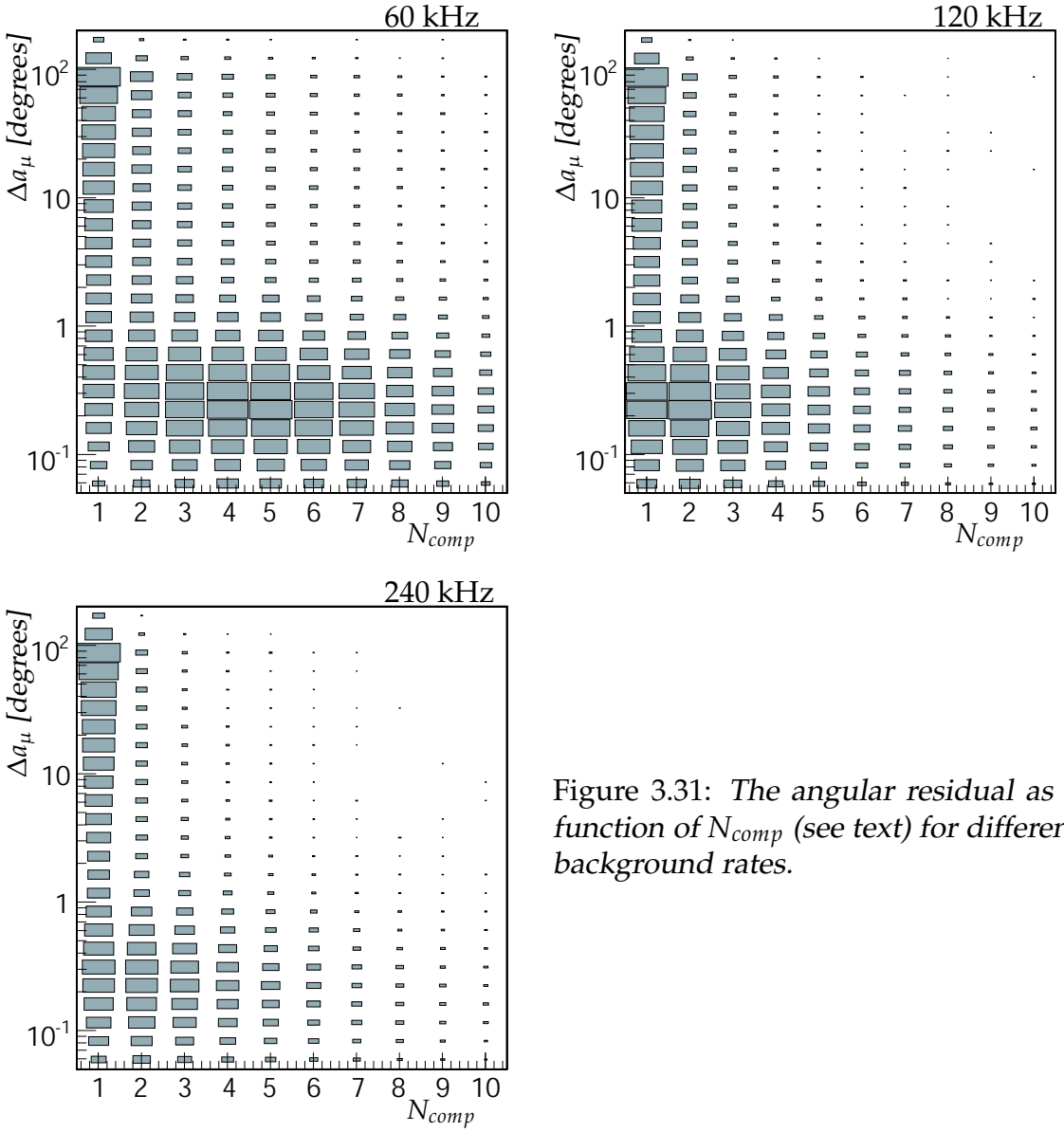

Figure 3.31: *The angular residual as a function of N_{comp} (see text) for different background rates.*

0.5 degrees for neutrinos at 60 kHz background rate and 1 degree at 240 kHz. However, in order to achieve better performance in terms of angular resolution, a more detailed modeling of the processes leading to the photon signal is needed. This was done by including a maximum likelihood fit using a detailed PDF for the hits. The PDF describing the hits was modified together with a the selection of hits in order to reduce the effect of correlations between hits. The maximum likelihood fit improves the angular resolution. It was found that the occurrence of correlated hits due to electro-magnetic showers affects the ability of the algorithm to estimate the track parameters. Several quantities were identified which can be used as indicators of track quality. The hit selection procedure based on the directional causality relation offers a way to calculate a track length. The angular resolution scales with this track length and is limited by the finite size of the Antares detector. The value of the log-likelihood per degree of freedom can be used to select a track from the track candidates. It is also a good measure of track quality. Also the number of tracks converging to the same solution is a measure of track quality. Studies of the performance of the track reconstruction were done for several background rates covering those encountered during data taking. The angular resolution is most affected at low energies. At 100 GeV muon energy doubling the background rates from 60 to 120 kHz or from 120 to 240 kHz results in a maximum deterioration of the angular resolution by a factor 2. However, at higher energies (10^6 GeV muon energy) the difference is negligible.